Mao *et al. Chem Synth* 2023;3:26
DOI: 10.20517/cs.2022.41

Chemical Synthesis

Review

Open Access

Check for updates

Recent advances in heavily doped plasmonic copper chalcogenides: from synthesis to biological application

Qiulian Mao[#], Jicun Ma[#], Mei Chen, Shiying Lin, Noman Razzaq, Jiabin Cui[*]

The Center for Molecular Imaging and Nuclear Medicine, State Key Laboratory of Radiation Medicine and Protection, School for Radiological and Interdisciplinary Sciences (RAD-X) and Collaborative Innovation Center of Radiological Medicine of Jiangsu Higher Education Institutions, Soochow University, Suzhou 215123, Jiangsu, China.
[#]Authors contributed equally.

[*]**Correspondence to:** Prof. Jiabin Cui, The Center for Molecular Imaging and Nuclear Medicine, State Key Laboratory of Radiation Medicine and Protection, School for Radiological and Interdisciplinary Sciences (RAD-X) and Collaborative Innovation Center of Radiological Medicine of Jiangsu Higher Education Institutions, Soochow University, 199 Renai Road, Industrial Park, Suzhou 215123, Jiangsu, China. E-mail: jiabin.cui@suda.edu.cn

How to cite this article: Mao Q, Ma J, Chen M, Lin S, Razzaq N, Cui J. Recent advances in heavily doped plasmonic copper chalcogenides: from synthesis to biological application. *Chem Synth* 2023;3:26. https://dx.doi.org/10.20517/cs.2022.41

Received: 15 Dec 2022 **First Decision:** 7 Feb 2023 **Revised:** 15 Apr 2023 **Accepted:** 26 Apr 2023 **Published:** 26 May 2023

Academic Editor: Bao-Lian Su **Copy Editor:** Dong-Li Li **Production Editor:** Dong-Li Li

Abstract

Copper-based chalcogenide compounds have emerged as alternative materials to Cd- or Pb-based traditional semiconductors and have drawn significant attention. Compared with widely reported semiconductors, copper chalcogenide nanocrystals (NCs) with abundant copper defects and vacancies present p-type features. Additionally, the migration of free hole carriers in copper-based chalcogenide NCs produced a metal-like local surface plasmon resonance (LSPR) effect. In this review, we focused on the plasmonic copper chalcogenide NCs achieved through a heavily doped strategy. The copper sulfur compounds with versatile atomic ratios and complex crystal structures exhibit rich electrical, optical, and magnetic properties, making them highly promising for a broad range of applications, from energy conversion to biomedical fields. Therefore, our main focus is on the classification of copper chalcogenide synthesis strategies, theoretical studies of doping, doping strategies, and biological applications. We aim to analyze the trends of copper-based chalcogenide nanomaterials for clinical applications by summarizing previous studies and presenting designs and concepts in a brief manner.

Keywords: Heavily doping, copper chalcogenides, LSPR, *in vivo* imaging, diagnosis and therapy

INTRODUCTION

Colloidal semiconductors with tunable size, morphologies, and compositions ranging from hundreds to thousands of atoms exhibit unique physical, optical, and electronic properties[1-3]. Over the past few decades, numerous colloidal semiconductors have been reported to address challenges related to environmental, healthy, and energy challenges. However, their efficacy has gradually weakened[4,5]. To date, various strategies have been used to enrich the properties of colloidal semiconductors[6,7], including doping, coupling, and modulation (epitaxial or nonepitaxial growth) methods for tunable bandgap engineering. This has resulted in superior electronic and optical properties and led to diverse applications in areas such as solar energy harvesting, imaging, display, and biological sensing.

Copper is an abundant metal with low toxicity, lower costs, and environmental compatibility, while copper chalcogenide semiconductors present a wide variety of compositions, sizes, and crystal structures[8-10]. This extremely versatile set of ingredients offers not only analogous properties to Cd- and Pb-based chalcogenide colloidal semiconductors but also possesses unparalleled features compared to the conservative nanocrystals (NCs), particularly in terms of photothermal and plasmonic properties[11-14]. Moreover, the synthesis protocol for colloidal copper chalcogenide NCs is still largely underdeveloped and does not yet reach the same level as traditional Pb- or Cd-based chalcogenides[15-19], which are still worthy of merit attention[20-24].

The copper atom has high reaction activity and a fast diffusion rate, making it easy to be oxidized and form monovalent or divalent copper ions. This leads to the formation of abundant defects in the lattice and different components with special properties, including the plasmonic feature observed in heavily doped copper-based chalcogenides. Compared with the noble metals (with a high density of free electrons and exhibiting strong light-matter interaction properties)[25-27] and n-type plasmonic semiconductors[28], heavily doped copper-based chalcogenides (including exotic-doping and self-doping)[22,29-33] present p-type features with a lower density of free charge carriers[34-36], resulting in longer wavelength LSPR absorption. Based on the above-described properties, plasmonic Cu-chalcogenide NCs have attracted significant attention due to their various applications, including the hotspot research field, such as copper-based radioimmune therapy and cuproptosis.

Inspired by the aforementioned potential applications, in this review, we summarize the recent advances in the heavily doped colloidal Cu-chalcogenide from synthesis to biological applications. Firstly, we provide a brief introduction of classifications for copper chalcogenide NCs and discuss the extensively reported synthesis methods. Next, we present theoretical studies based on doped plasmonic Cu-chalcogenide NCs with LSPR properties. We also review the doping strategies for the formation of doped Cu-chalcogenide NCs. Subsequently, we discuss the wide range of applications for colloidal plasmonic Cu-chalcogenide NCs, including biosensing, *in vivo* imaging, diagnosis, and cancer therapy. Finally, we provide insights into the opportunities and challenges of these potential applications for the next generation.

CLASSIFICATION OF COPPER CHALCOGENIDE NCS AND SYNTHESIS STRATEGY

The copper chalcogenide compounds were initially discovered in minerals, which is why most of them are named Chalcocite, Djurleite, Roxbyite, Digenite, Anilite, and Covellite. For bulk Cu_2S crystals, the band gap is 1.2 eV[37-40]. However, the one-valence copper atom is readily oxidized by the oxygen in the air, which leads to the formation of the $Cu_{2-x}S$ ($x = 0 \sim 1$) compound along with a copper vacancy, resulting in the p-type feature. In Figure 1, the number of copper vacancies is one of the main factors for the formation of diverse $Cu_{2-x}S$ crystal structures, including *hexagonal*, *cubic*, *monoclinic*, and *orthorhombic* crystal structures. Simultaneously, the rearrangement of the S atom (usually very slow) during the crystallization results in the formation of numerous metastable stages, such as chalcocite (Cu_2S), djurleite ($Cu_{1.94}S$), roxbyite ($Cu_{1.81}S$),

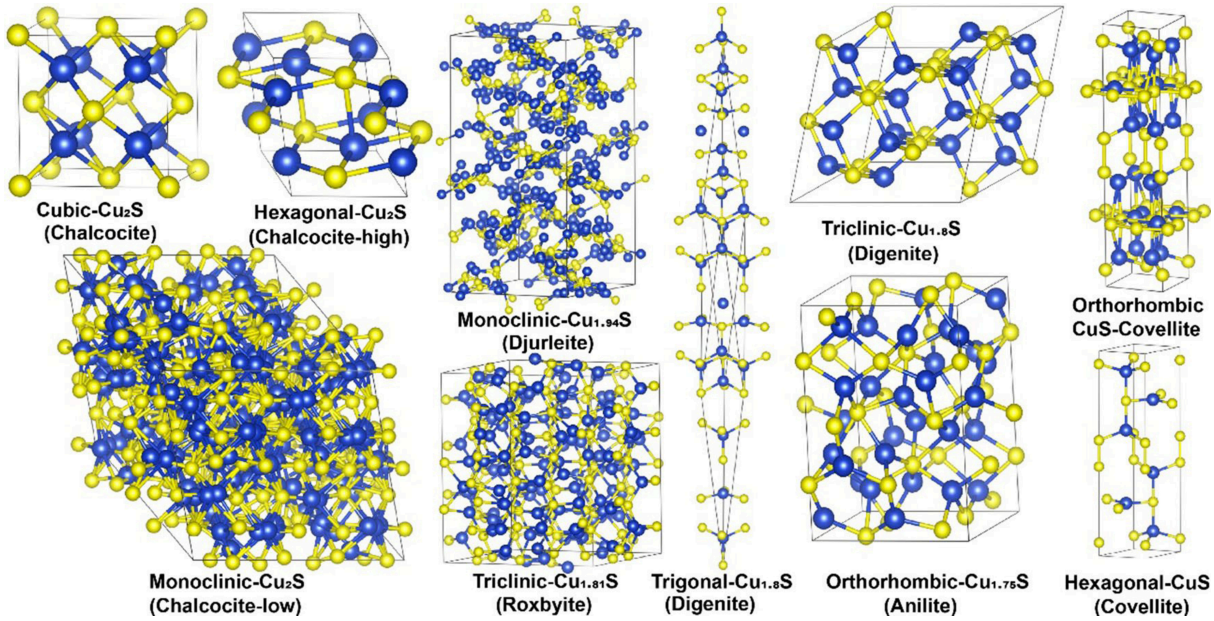

Figure 1. Crystal structure model of the Chalcocite, Djurleite, Roxbyite, Digenite, Anilite, and Covellite. Sulfur and Copper atoms are marked in yellow and blue, respectively.

digenite ($Cu_{1.8}S$), anilite ($Cu_{1.75}S$), and covellite (CuS), as shown in Table 1. Additionally, the similar chemical properties of anion elements result in a wide range of materials for $Cu_{2-x}E$ (x = 0~1, E = S, Se, or Te). The structural and compositional diversity of copper chalcogenides creates challenges for precisely controlled synthesis and enriches the fabrication method used.

The classical method for forming the NCs involves the "bottom-up" and "top-down" strategies. As for the colloidal copper chalcogenides, we usually use the organic synthesis method, which includes the "hot-injection" and "heat-up" technologies[60,61]. The process involved first preparing the copper compounds as a precursor. Then, the flask containing the organic solvent was heated to a high temperature, and the precursor was quickly injected. The primary stage after the injection is the boom of the nucleation. The reaction then proceeds quickly into the crystallization and growth stage. Over time, the Ostwald ripening occurs[62]. Therefore, achieving desirable colloidal nanocrystals requires precise control of activity and amount of the precursor, organic solvent, reaction temperature, and time. Omitting any of these factors could affect the outcome. The traditional Cd- or Pb-based colloidal semiconductor has been well-studied and applied in various ways. However, the synthesis technologies for copper chalcogenides have not yet reached the same level as those for the Cd- or Pb-based protocols. As a result, numerous research work for the irregular shape of copper chalcogenides is fabricated with the cation exchange method. However, it is worth noting that the precisely controlled synthesis strategy for copper chalcogenides remains challenging and has significant room for development.

THEORETICALLY STUDIES FOR DOPING CU-CHALCOGENIDES NCS

LSPR feature was first observed in the "Lycurgus Cup", which was made of colloidal gold particles for drinking. To date, the LSPR properties of the colloidal NCs have been widely used in diverse applications, including biosensing, luminescence, and therapy.

Table 1. The summary of the different types of the copper chalcogenides

Materials	Crystal system	Space group	Mineral name	Reference
Cu_2S	Hexagonal	$P6_3/mmc$ {194}	Chalcocite-High	[41-44]
Cu_2S	Cubic	Fmm {225}	Chalcocite	[39,45]
Cu_2S	Monoclinic	$P2_1/c$ {14}	Chalcocite-Low	[46]
$Cu_{1.94}S$	Monoclinic	$P2_1/c$ {14}	Djurleite	[47-49]
$Cu_{1.81}S$	Triclinic	P {2}	Roxbyite	[50]
$Cu_{1.8}S$	Trigonal	Rm {166}	Digenite	[51]
$Cu_{1.8}S$	Triclinic	P{2}	Digenite	[47,52-54]
$Cu_{1.75}S$	Orthorhombic	Pnma {62}	Anilite	[55,56]
CuS	Hexagonal	$P6_3/mmc$ {194}	Covellite	[57,58]
CuS	Orthorhombic	Cmcm {63}	Covellite	[57,59]

Generally, the LSPR feature occurred when the frequency of the irradiated light matched well with that of the inherent oscillation frequency of the substrate (usually determined by the density of the free charge carrier, the free electron, or the hole), leading to significant amplitude enhancement, also called "resonance". This phenomenon is typically observed in noble metal colloidal nanocrystals (especially Au and Ag), which have a large number of free electrons in the conduction band. As shown in Figure 2A, the LSPR feature depends on the density of the free carrier, with lower carrier density leading to long-wavelength resonance absorption and vice versa. In addition, the symmetry of the colloidal NCs usually results in various surface distributions of the free carrier. Regarding the isotropy crystals (spherical or quasi-spherical NCs), the surface oscillation is the same and shows a single LSPR absorption peak. For this reason, the absorption peaks of the colloidal gold and silver NCs localized at 520 and 480 nm, respectively. As for the anisotropy crystals, the surface distribution of the free carriers is significantly different, leading to the splitting of the LSPR absorption peak. According to Figure 2B, the difference between the longitudinal and transverse electrons oscillation of gold nanorods causes two LSPR absorption peaks: one localized at 520 nm and another determined by the aspect ratio.

The LSPR feature mentioned above is focused on the noble metal colloidal NCs. The density of the free carrier for the intrinsic semiconductor is usually much lower than that of the metal NCs. Thus, there is no distinct LSPR absorption peak for intrinsic semiconductors. It is generally assumed that the LSPR behavior of the semiconductor NCs is caused by collective oscillations of superfluous free carriers in the lattice related to the constituent vacancies and the ionized dopant impurities[63-65]. Therefore, the doping strategy plays a remarkable role in the tuning of the density of free carriers bringing about the observation of the plasmonic n-type or p-type doped-semiconductor in Figure 2C. In this study, we will briefly discuss the calculation study model for the doped plasmonic semiconductor.

Theoretical studies of spherical or quasi-spherical plasmonic materials have primarily relied on the Drude model, which has been widely discussed in the literature. In this context, we emphasized the significance of the anisotropy of plasmonic materials. For example, in the case of the plasmonic copper chalcogenides nano-disks or rods, the calculation function of LSPR absorption "*A*" is shown below:

$$A \propto \omega \cdot \varepsilon_m \sum_i \left(\frac{(1/P_i^2)\cdot \varepsilon_2}{(\varepsilon_1 + \frac{1-P_i}{P_i}\varepsilon_m)^2 + {\varepsilon_2}^2} \right) \quad (1)$$

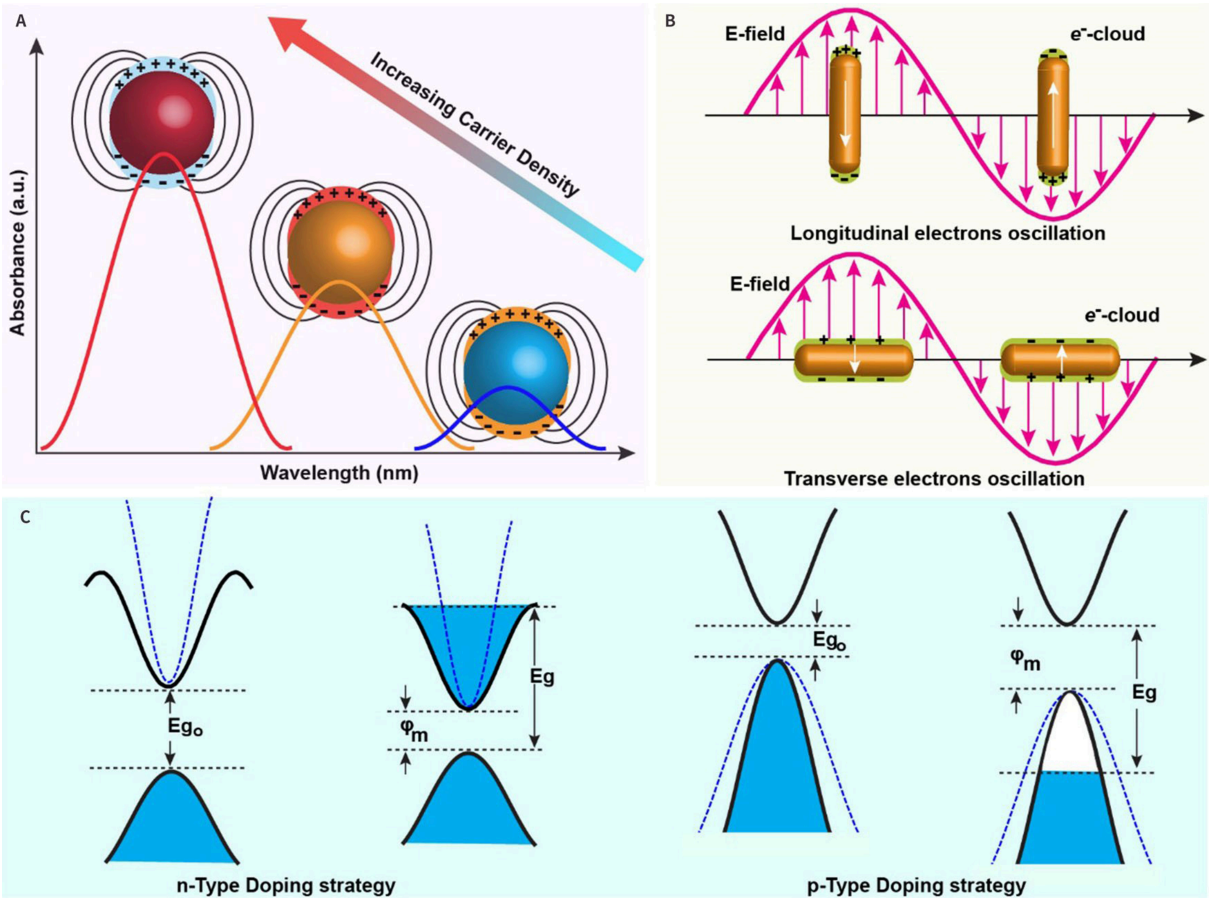

Figure 2. The Drude model for plasmonic materials. (A)-(B) The longitudinal and transverse electrons oscillation; (C) The theoretical diagram of n-Type Doping strategy and p-Type Doping strategy.

Here, ω is the angular frequency of the incident light. ε_m is the dielectric constant of the medium. ε_1 is the real part of the dielectric constant of NPs. ε_2 is the imaginary part of the dielectric constant of NCs. P is the function of the axis (a is the long axis, and b and c are symmetric). Then the polarization factors are known as below:

$$P_a = \frac{(1-s^2)}{s^2}\left[\frac{1}{2s} \cdot ln\left(\frac{1+s}{1+s}\right) - 1\right] \quad (2)$$

$$P_b = P_c = \frac{1-P_a}{2} \quad (3)$$

Here, s is the geometric parameter of the NCs and is defined in the equation (4):

$$s = \sqrt{1 - (\frac{1}{R})^2} \tag{4}$$

Where R is the aspect ratio of the rod. In turn, according to the Drude theory, $\varepsilon(\omega)$ could be expressed as:

$$\varepsilon(\omega) = \varepsilon_1 + i\varepsilon_2 = 1 - \frac{\omega_p^2}{\omega^2 + i\gamma\omega} \tag{5}$$

Where γ is the collision frequency (similar/to the high line wide). And $_p$ the bulk plasma frequency can be defined as below:

$$\omega_p = \sqrt{\frac{{N_e}^2}{\varepsilon_0 \cdot m_e}} \tag{6}$$

Where N is the free carrier density. m_e is the mass of the electron. ε_0 is the permittivity of the free space. Thus the collision frequency can be expressed as:

$$\gamma = \frac{1}{\tau} = \frac{e^2}{\sigma \cdot m_h} \tag{7}$$

Where m_h is the mass of the hole. e is the elementary charge. σ is the conductivity of NCs ($Cu_{1.8}S$: $2.4 \times 10^3\ \Omega^{-1} \cdot cm^{-1}$). Then the real part ε_1 and imaginary part ε_2 of the dielectric constant for copper chalcogenides nano-disks or rods could be calculated as:

$$\varepsilon_1 = 1 - \frac{\omega_p^2}{\omega^2 + \gamma^2} \tag{8}$$

$$\varepsilon_2 = \frac{\omega_p^2 \cdot \gamma}{\omega^3 + \gamma^2 \omega} \tag{9}$$

In short, the precise calculation for the doped copper chalcogenides with an anisotropy shape is still challenging, leaving a large space for further investigation.

DOPING STRATEGY

The carrier density is a major parameter that determines the LSPR properties[66-68]. Therefore, the LSPR feature could be manipulated in a controllable manner with shapes, size, and surface properties that determined the distribution of free charge carriers or other strategies to tune the density of the carriers, including the light or electronic doping. We will discuss these details in the following paragraph.

Electronic doping

Electronic doping is an effective method for the dynamic regulation of plasmonic materials[69-71]. For example, Ou *et al.* reported an electrochemical lithiation process for forming the doped plasmonic $Cu_{2-x}Se$ nanocrystals with dynamic and reversible operation[70]. As described in Figure 3A, the valence state of Se was reduced from intermediate states to -2 after the electron injection operation. On top of this, the hole concentration was dramatically decreased, which made the Fermi energy level of NCs change from the initial value of -0.82 eV to -0.39 eV. In contrast, during the discharged process, the Fermi energy level drops, and the band gap returns to the initial level of -0.82 eV, as shown in Figure 3B and C.

Photo-induced LSPR modulation

$Cu_{2-x}S$ reveals strong LSPR features within the near-infrared (NIR) region (800-1800 nm), which are determined by the concentration of the copper vacancy generated through the self-doping method. Using a photo-reduction process[70-72] to manipulate the free hole density, researchers developed a simple strategy for fabricating plasmonic $Cu_{2-x}S$ NCs. Alam *et al.* have successfully modulated the LSPR feature of $Cu_{2-x}S$ NCs through the photochemically generated radicals $MV^{+\bullet}$[73]. The electron transfer is reversible through the changed procedure, as shown in the infrared LSPR absorption spectra presented in Figure 4A and B. The possibility of controlling LSPR by electron donors generated by photochemical protocols can be further stretched to create optical windows in the infrared region. Additionally, it is also possible to achieve the LSPR properties of $Cu_{2-x}S$ NCs with the assistance of a semiconductor in a photoreduction reaction. Interestingly, when the Fermi level underwent equilibration with electron transfer, there was an increase compared to the unequilibrated state, leading to a reduction of the NIR LSPR feature, as demonstrated in Figure 4C. The reversibility of electron transfer through LSPR response is probed and shown in Figure 4D.

Morphology and surface ligands effect for LSPR

Different shapes of the synthesized nanomaterials will lead to distinct LSPR features and generate interesting optical properties. The LSPR feature in the near-infrared region has been confirmed in self-doped $Cu_{2-x}E$ (E = S, Se and Te) semiconductor NCs due to the existence of free holes related to Cu vacancies in the lattice[74-77].

To date, plasmonic NCs have been developed by changing the composition, morphology, or surface ligands of NCs[68,78,79]. Li *et al.* exhibited a strategy to synthesize high-quality copper telluride nano-cubes, nanoplates, and nanorods. Figure 5A-C showed the morphology of the CuTe NCs through the high-resolution transmission electron microscope (HRTEM) micrographs obtained. The corresponding absorption spectra of copper telluride with different shapes were shown in Figure 5D. In the spectra obtained from CuTe nano-cubes, a strong absorption band centered at 900 nm and associated with LSPR is clearly observed. At the same time, weak absorption intensity in UV-Vis-NIR spectra and almost vanishing NIR absorption characteristics were observed in CuTe nanoplates and nanorods, respectively. This may be caused by the small size of the fine nanorods not supporting detectable plasma[80]. The synthesis procedure involved the reaction of a copper salt with trioctylphosphine telluride precursor in the presence of lithium bis-(trimethylsilyl)amide and oleylamine (OAm).

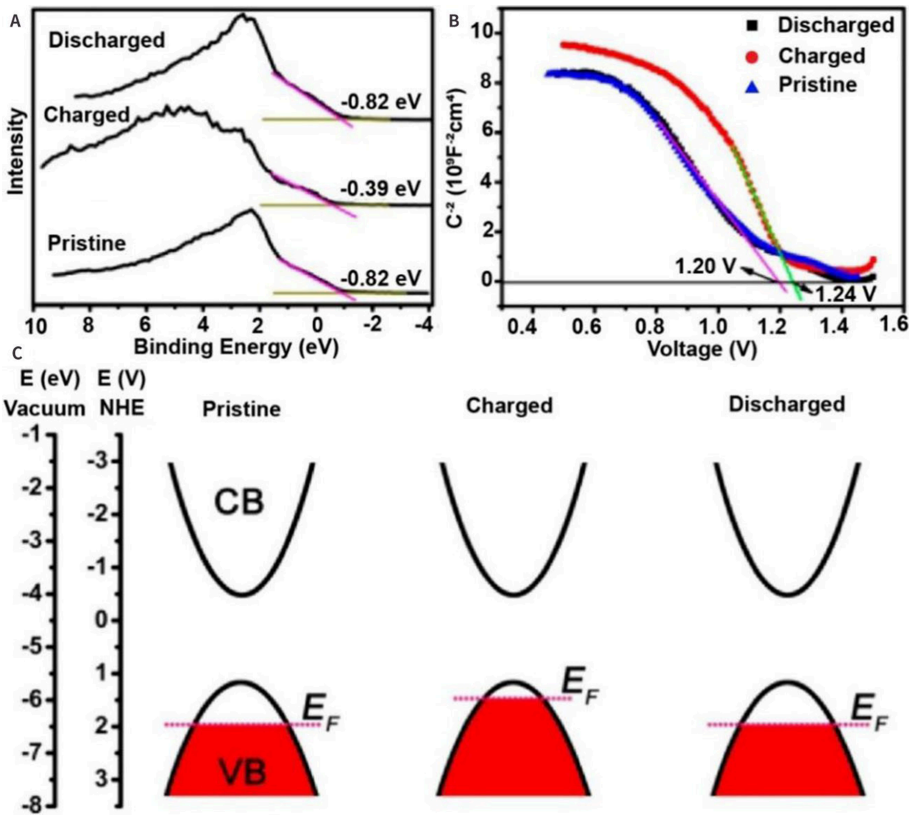

Figure 3. (A) Valence band spectra of $Cu_{2-x}Se$ NPs and (B) Mott-Schottky diagram; (C) Schematic diagram of energy band diagrams in newly deposited (pristine), lithiated (charged), and fully delithiated (discharged) states[70]. Copyright © *American Chemical Society* 2018.

Similarly, the carrier density surface treatment could also be utilized for the formation of the plasmonic copper chalcogenides NCs, as illustrated in Figure 5E[68]. The TEM micrographs in Figure 5F and G showed copper sulfide NPs. The attained tetradecahedrons and nano-disks have similar $Cu_{31}S_{16}$ phases; however, they presented different optical properties, as shown in Figure 5H. The nano-disks produced without Sn^{4+} treatment exhibited a strong LSPR absorption in the NIR region because of the collective oscillation of free charge carriers. In sharp contrast, the plasmonic feature was diminished with the Sn^{4+} treatment. This suggested that Cu vacancies or trapped free charge holes could be efficiently filled by trace amounts of Sn^{4+} [81]. The dramatic change of the LSPR peak is due to the phase transition, as shown in Figure 5I. Specifically, a higher density of copper vacancies results in a blue shift of the LSPR peak, a higher absorption intensity, a narrower bandwidth, and an increase in bandgap absorption[82]. The main factors that trigger the phase transition are the generation of copper vacancies and the rearrangement of Cu cations and S anions[83].

Chen *et al.* demonstrated that the Sn^{4+} could direct the evolution of djurleite $Cu_{31}S_{16}$ from nano-disk to tetradecahedron in the *c*-axis orientation[68]. The $Cu_{31}S_{16}$ NCs were transformed into more copper-deficient Cu_7S_4 NPs by heat treatment with amine-functional ligands. The roxbyite Cu_7S_4 NPs demonstrated a stronger and shorter LSPR peak while retaining the shape of the djurleite $Cu_{31}S_{16}$ NPs. Swihart *et al.* also reported that the conversion of CuS and Cu_2S was possible through heat treatment in various organic reagents after surface treatment[79].

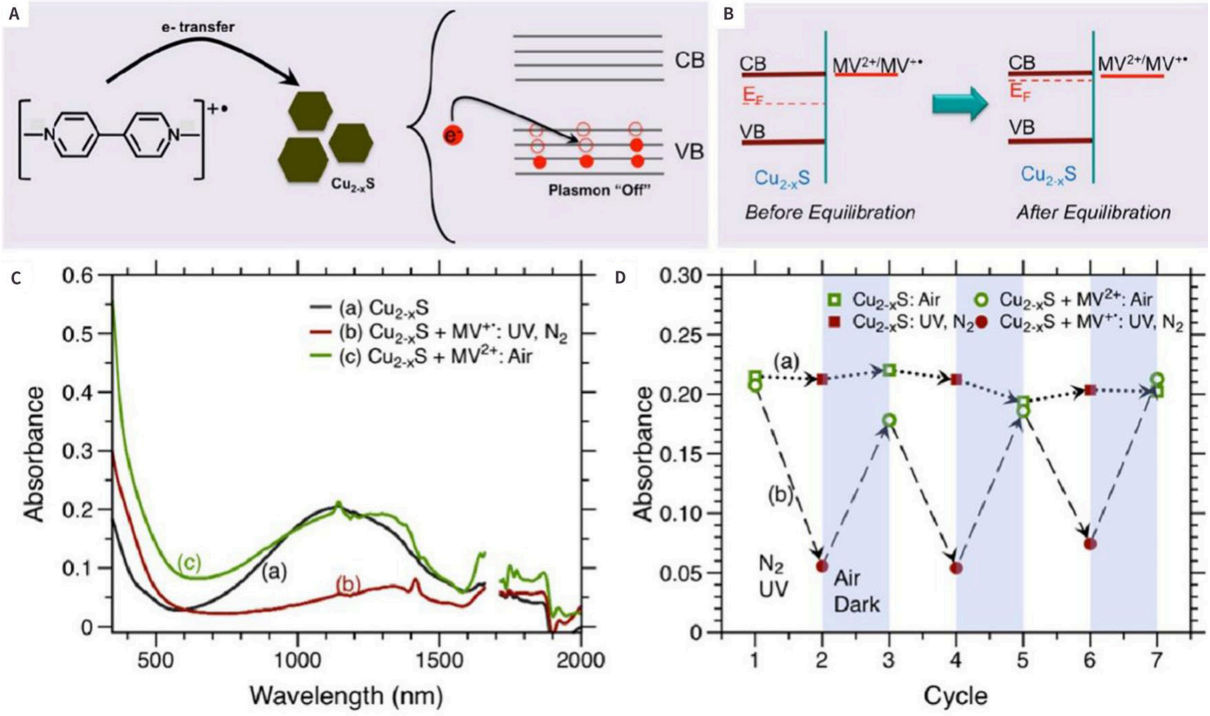

Figure 4. (A) Electron transfer process under inert atmosphere from $MV^{+\bullet}$ to $Cu_{2-x}S$; (B) Fermi level equilibration between $Cu_{2-x}S$ Nanocrystals and $MV^{2+}/MV^{+\bullet}$ Redox Couple; (C) The absorption spectra, and (D) Electron transfer through LSPR response[73]. Copyright © *American Chemical Society* 2016.

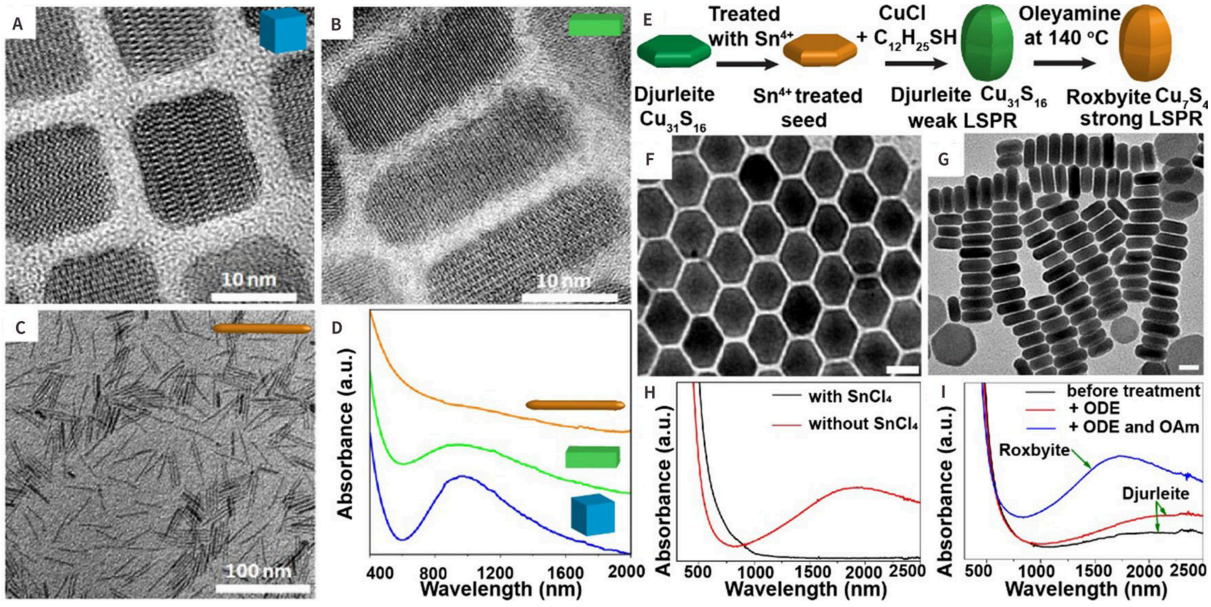

Figure 5. TEM micrograph of CuTe NCs: (A) nano-cubes; (B) nanoplates and (C) nanorods, and (D) absorption spectra of CuTe nano-cubes, nanoplates, and nanorods[80]; (E) Schematic diagram of reaction mechanism with surface treatment, TEM images of CuS NPs synthesized with (F) and without (G) 1.0 mmol $SnCl_4$, (H) UV-vis-NIR absorption spectra of CuS NPs; and (I) UV-vis-NIR absorption spectra of $Cu_{31}S_{16}$ tetradecahedrons[68]. (A)-(C): Copyright © *American Chemical Society* 2013; (D)-(F): Copyright © *American Chemical Society* 2016. TEM: transmission electron microscope.

Hybrid structure

Heavily-doped semiconductor nanometer materials also exhibit strong LSPR absorbance when combined with the plasmonic metal NCs. The copper chalcogenides have promising potential for use in photothermal therapy (PTT)[84-86] applications. Zhu *et al.* and Liu *et al.* synthesized Au-$Cu_{2-x}Se$ nanocrystals, which combined heavily doped p-type semiconductor and noble metal domains[85,87]. They reported a novel type multiphase nanoparticles (NPs) consisting of a heavily doped p-type $Cu_{2-x}Se$ and an Au domain (n-type feature), as shown in Figure 6A and B. This nanocrystal exhibited a broad LSPR absorption region across visible to NIR absorption wavelengths and demonstrated strong interactions between the two nanocrystal domains[87], as depicted in Figure 6C.

BIOLOGICAL APPLICATION

The particular applications of NPs have attracted increasing attention from scholars with the speedy development of nanotechnology, materials science, and molecular imaging. They have brought great convenience for us to observe the situation in real-time *in vivo* as a clinical detection and research tool. As type of nanomaterial, contrast agents can visualize the physiological structures in organisms. In recent years, researchers have found that nanomaterials can provide high-resolution and high-contrast images for the visualization of precision medicine delivery, which plays a crucial role in imaging applications. Among them, copper-based chalcogenide compounds present unique advantages with strong NIR LSPR absorption feature[74], attracting significant attention for photothermal-guided biological applications[88-90]. There are several strategies to improve photothermal conversion efficiency. (1) Changing the carrier concentration the doped semiconductor[91] to increase the possibility for non-radiation transition (usually released as heat energy). (2) Manipulating the crystal phase, morphology, and particle size of $Cu_{2-x}S$ nanocrystals to modify the LSPR absorption feature[92]. (3) Forming the hybrid structure by increasing the cross-section absorption[93].

In this direction, we describe the application of copper chalcogenide NCs from biosensing to *in vivo* imaging and therapy. The main *in vivo* imaging functions of nano-copper sulfide include computed tomography (CT), magnetic resonance imaging (MRI), single-photon emission computed tomography (SPECT)/CT, fluorescence imaging (FLI), and PA imaging. Some researchers enhanced copper chalcogenide NCs with fluorescent molecules, such as indocyanine green (ICG), and luminous nanoparticles, such as quantum dots (QDs), upconversion nanoparticles, and radioactive isotopes. These enhancements may provide additional imaging choices. The utilization of copper sulfide NCs in tumor therapy includes PTT, chemodynamic therapy (CDT), photodynamic therapy (PDT), immunotherapy (IT), radiation therapy (RT), and multimodal combination therapy. Most of the treatment strategy is mainly based on the response of nanomaterials to stimuli, which can elicit an immune response and attract apoptosis or death of tumor cells.

Biosensing

Heavily-doped copper chalcogenides, as p-type plasmonic materials, were wildly used in biosensing. In the past few decades, copper chalcogenides have attracted significant attention due to their unique characteristics as both metals and semiconductors[94-97]. Several studies have proven that $Cu_{2-x}S$ exhibited broad-band LSPRs in the NIR region and fundamentally altered light-matter interactions. These characteristics have led to a wide range of applications, including enhanced spectrum[98], sensing[99], photocatalysis[100,101], and optical devices[102].

In Figure 7A, Zhou *et al.* reported a core-shell composite material named $mCu_{2-x}S@SiO_2@-Y_2O_3:Yb^{3+}/Er^{3+}$ for the fingerprint recognition. As shown in Figure 7B, the color of the material changed from green to orange with increasing excitation power. This study opened up new ideas for the design and preparation of

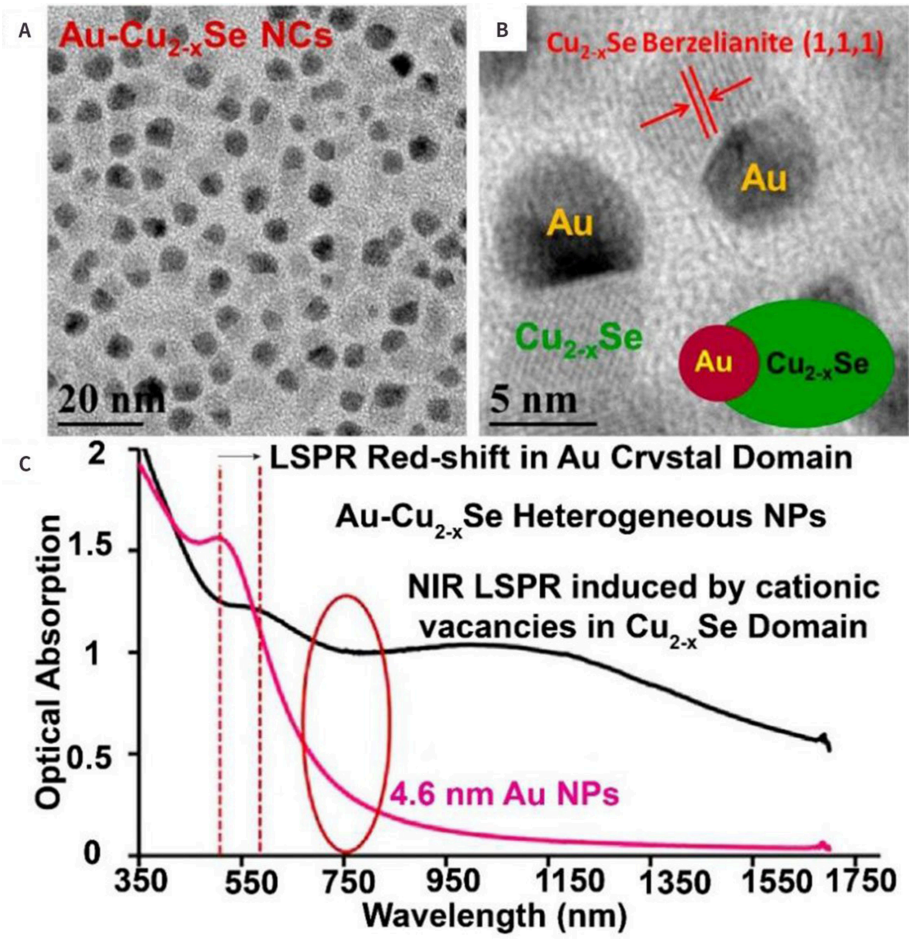

Figure 6. TEM (A). and HRTEM; (B) of Au-$Cu_{2-x}Se$; (C) Optical absorbance of Au NPs (red) and Au-$Cu_{2-x}Se$ heterodimer NPs (black)[87]. Copyright © *American Chemical Society* 2013. HRTEM: high-resolution transmission electron microscope; TEM: transmission electron microscope.

upconversion core-shell structures of semiconductor plasmonic nanoparticles. It provided a reference for the application of upconversion nanocrystals (UCNPs) and semiconductor plasmonic nanoparticles in photonics[103]. Another group, Cui *et al.*, also designed and synthesized high-efficiency photothermal semiconductor nanocomposites for potential fingerprint photothermal imaging[104]. They used a novel method to synthesize Cu_7S_4 NCs with good photothermal properties and fabricated amphiphilic nanocomposites with good affinity by coating Cu_7S_4 nanoparticles with allyl thiol polymerization, as shown in Figure 7C and D. Due to the high photothermal conversion efficiency of Cu_7S_4 NCs, they were developed as a simple and versatile photothermal latent fingerprints (LFPs) imaging method, which was demonstrated to be effective for imaging of LFP residual on different substrates (different background colors), as shown in Figure 7E. It would be very helpful for crime scene investigation. In addition, it was produced, and the dual-mode fluorescence-photothermal imaging techniques were used to monitor trinitrotoluene, the integrated photothermal image of LFPs.

In vivo imaging

Over the past few decades, nanomaterials have led to the rapid development of emerging *in vivo* imaging techniques. The close collaboration between chemists and imaging scientists plays a decisive role in the application of emerging nanomaterials to solve difficult clinical problems. The application of nanomaterials

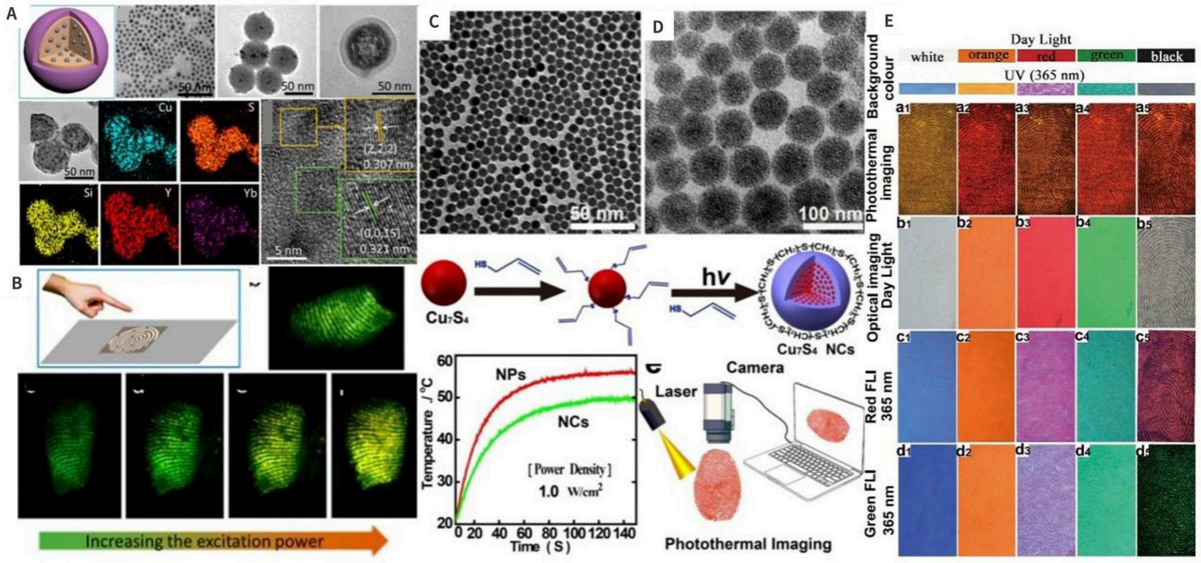

Figure 7. Applications of copper sulfur compounds in biosensing. (A) The TEM characterization of $mCu_{2-x}S@SiO_2@Y_2O_3:Yb^{3+}/Er^{3+}$ and the application of fingerprint recognition in (B)[103]; (C) and (D) TEM images of hydrophobic Cu_7S_4 NPs and amphiphilic Cu_7S_4 NCs included fabrication strategy for Cu_7S_4 NCs and photothermal effects of Cu_7S_4 NCs under a given power density versus the irradiation time, and scheme for photothermal imaging of fingerprints. (The photothermal tests were conducted on the thin film of Cu_7S_4 NC powder with excitation at 808 nm); (E) the photothermal latent fingerprints imaging method[104]. (A)-(B): Copyright © *American Chemical Society* 2017; (C)-(E): Copyright © *American Chemical Society* 2015.

in imaging technology not only improves diagnostic sensitivity and specificity but also increases the range of contrast agents, making nanomaterials a dominant tool for molecular imaging capabilities. In addition, nanomaterials make imaging much easier. While many recent articles have discussed the conveniences of nanomaterials for imaging applications, they only focus on sub-categories such as disease-specific applications or cell-specific applications. We rearrange the imaging methods according to the order of clinical use as follows.

Computed tomography

Computed tomography (CT) technology plays a compelling role in the clinic due to its high spatial resolution; however, it is still restricted by the related radiation burden and a lack of individual tissue specificity. Cui *et al.* reported a plain strategy to form a Cu_7S_4-Au hybrid structure based on heavily doped Cu_7S_4 NCs, resulting in strong LSPR absorption at approximately 808 nm[105]. Based on this, the ^{19}F molecules were bonded on the surface of the hybrid structure by click chemistry to form Cu_7S_4@Au@PSI-^{19}F nanoparticles (named as CNs) in Figure 8A. These NCs were successfully used for coinstantaneous CT/^{19}F-MRI guided PTT with low background signal and strong penetration depth, as demonstrated in Figure 8B and C. Subsequently, the polymorphous CNs were utilized for the CT/^{19}F-MRI-guided PTT ablation of deep tumors. By connecting small gold domains with Cu_7S_4, the LSPR absorption of the CNs was converted to the *in vivo* transparent window, which significantly enhanced the efficacy of PTT and reduced the laser damage to healthy tissues. Another group, Wang *et al.*, prepared a $Cu_{2-x}Se/Bi_2Se_3$@PEG (named CB3@PEG) nanohybrid structure by the cation exchange method. The added Bi had a high X-ray absorption coefficient, making it a promising contrast medium for CT imaging[106], as shown in Figure 8D. As mentioned above, the synthesis pathways and mechanism diagram of CB3@PEG were shown in Figure 8D, and the adjacent photos showed the specific application of CB3 material in different imaging modalities *in vitro* or *in vivo*, mainly including PTT imaging in Figure 8E and F, CT imaging in Figure 8G and H, and MRI in Figure 8I-K. It also showed great potential for multimode synergistic therapy. Shi *et al.* designed and synthesized the

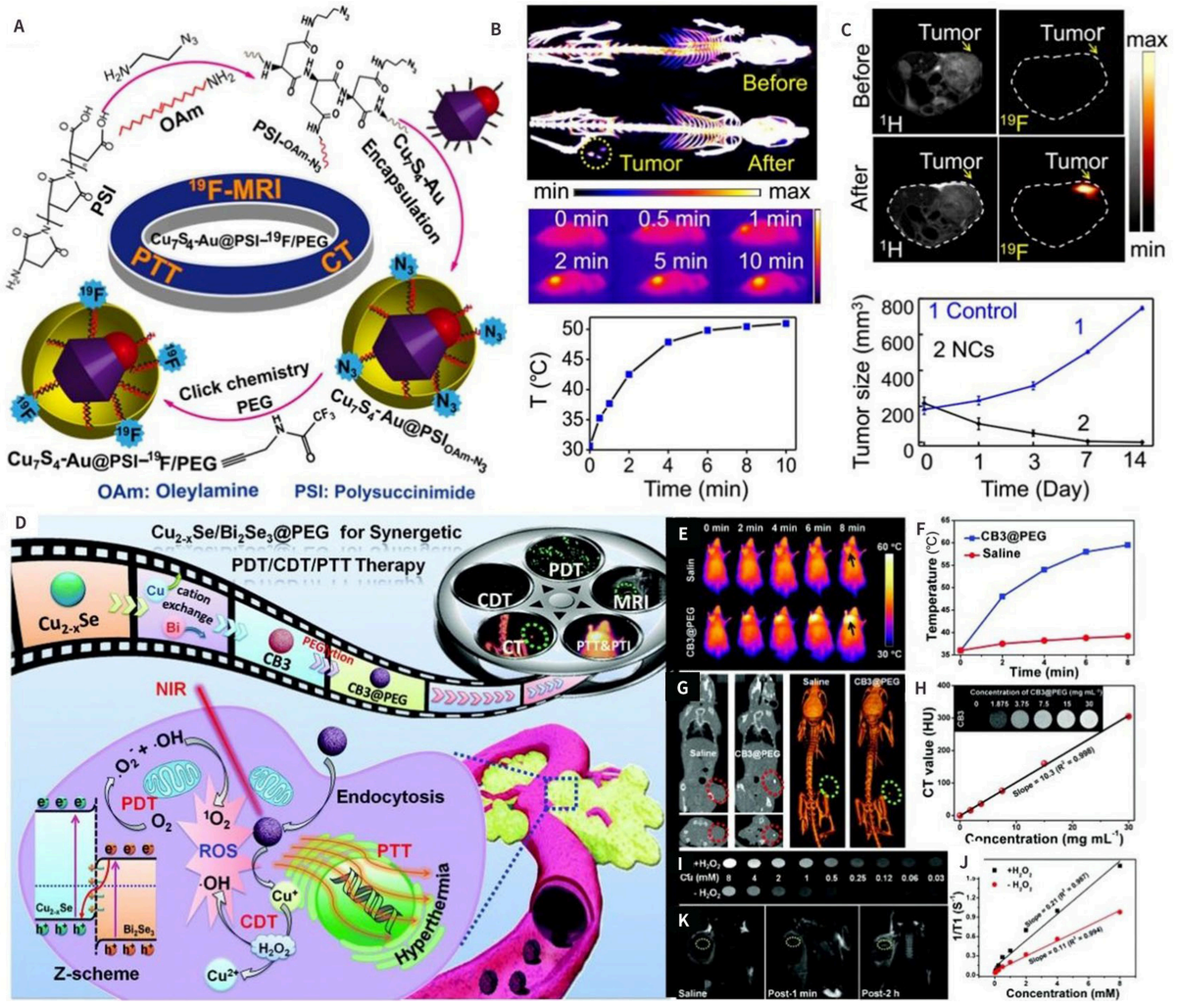

Figure 8. (A). Schematic representation of the synthesis of Cu_7S_4-Au@PSI-^{19}F/PEG and its application to imaging *in vivo*[105]; (B) CT and PAI imaging; and (C) MRI imaging in vivo; (D) Schematic representation of $Cu_{2-x}Se$ /Bi_2Se_3@PEG preparation; and (E) and (F) PAI (G) and (H) CT and (I), (J), and (K) MRI multimodal imaging-guided cancer diagnosis and treatment *in vivo*[106]. (A)-(C): Copyright © *American Chemical Society* 2018; (D)-(J): Copyright © *Royal Society of Chemistry* 2013. CDT: chemodynamic therapy; CT: computed tomography; MRI: magnetic resonance imaging; PDT: photodynamic therapy; PTI: photothermal imaging; PTT: photothermal therapy.

CuS nanoparticle named RGD-CuS-$Cy_{5.5}$, which demonstrated strong NIR fluorescence. And CT contrast medium can accurately distinguish metastatic sentinel lymph nodes (SLN) metastasis of gastric cancers, as mentioned earlier[107].

Magnetic resonance imaging

From another aspect, Magnetic resonance imaging (MRI) is one of the best commendable imaging techniques that can detect deeper soft tissues with inappreciable injury[108-110]. MRI provides more information than other imaging technologies in medical imaging and does not cause photo-agent allergy or ionizing radiation damage. Additionally, MRI has higher density resolution[111-113] than other imaging methods. Conventional ^{1}H MRI suffers from a low signal-to-noise ratio (SNR) because of the higher moisture content in the body. Cui *et al.* reported the polymorphous NCs, including the ^{19}F and Cu_7S_4-Au nanoparticles, for newly guided PTT using ^{19}F-MRI and CT imaging[105,114]. The background was negligible, and the MRI images were shown in Figure 8C. Another material, CB3@PEG nano-heterostructures, have

been prepared through a cation-exchange process by Wang *et al.*[106] Consequently, the affected Cu^{2+} regulates the single electron spin, revealing the T_1-weighted MRI ability sensitive to H_2O_2 concentration, as shown in Figure 8I-K.

Positron emission tomography

Positron emission tomography (PET) is a formidable biomedical imaging technique widely used for diagnosing clinical oncology due to its practicality and accurate susceptivity[115-117]. PET is one of the updated imaging mechanics that could show the metabolism of biomolecules, receptors, and neurotransmitter activity *in vivo*[118]. In addition, it has been widely used in differential diagnosis, efficacy evaluation, condition evaluation, new drug development, and organ function research. (1) High sensitivity. As we know, PET is an imaging technique that reflects molecular metabolism. When the disease occurs in the early stages of molecular level changes, the morphological and pathological changes in the damaged area may not yet be visible, and MRI and CT examinations cannot provide a clear diagnosis; however, PET inspection can identify the damaged area and provide 3D images and quantitative analysis to achieve early diagnosis. (2) High specificity. It is difficult to distinguish between benign and malignant tumors in organs by MRI and CT examinations; however, PET can be used as a diagnostic tool according to the high metabolism characteristics of malignant tumors. (3) Whole-body scan. PET can be used as a one-time whole-body examination to produce images of all parts of the body. (4) Good safety. The radionuclides required for PET examinations have a certain level of radioactivity, but the amounts used are negligible. Additionally, the radionuclides have a short half-life of approximately 12 minutes and a long half-life of approximately 120 minutes, ensuring a fast metabolism. After physical decay and biological metabolism, the contrast agent stays in the body for a short period of time. The dose of PET required for a whole-body examination is much lower than that of conventional CT examinations, so it is safe and reliable. ^{64}Cu was successfully applied *in vivo* imaging as an efficient PET luminescence. Guo *et al.* depicted a direct composite of intrinsic radioactive material by amalgamating ^{64}Cu directly into CuInS/ZnS nanostructures, using $^{64}CuCl_2$ as the synthesis precursor[119], as shown in Figure 9A. It clearly displayed characteristic whole-body coronal PET images of U87-tumor-bearing mice in Figure 9B. Zhou *et al.* developed a patented, chelator-free ^{64}Cu-CuS compound that can be used for PET imaging[120] and as a photothermal sensitizer for PTT in tumor ablation, as shown in Figure 9C-D. These ^{64}Cu-CuS compounds were easy to fabricate, exhibited exceptional stability, and allowed for almost noninvasive micro-PET imaging. In summary, the combination of smaller diameter, stronger absorption of NIR, and comprehensiveness of ^{64}Cu as a configurational constituent made these NPs well-suited for synergetic molecular imaging and therapy.

Although PET technology presents great success in the clinic, especially for early tumor diagnosis and therapy evacuation, there are still some disadvantages that cannot be ignored and limit its development. PET technology may not be effective in detecting early adenocarcinomas, especially ground glass nodules, as these may not exhibit active metabolism and will show negative results. Additionally, false positives can occur when infections, tuberculosis, sarcomatoid lesions, and other diseases are present, as these can show positive results. Furthermore, because radioactive isotopes must be injected into the body during the examination, PET has the disadvantage of exposing patients to a large amount of radiation, and it is absolutely prohibited for use in screening otherwise healthy individuals.

Fluorescence imaging

Fluorescence imaging (FLI) is particularly significant for qualitative preclinical applications[118]. As we know, FLI has lots of advantages, including simple synthesis, fluorescence signal visualization, and multiple marker sites. It is a consummate implement for imaging-guided angiography. Metal NCs have been vastly utilized in imaging techniques, including PET, MRI, and FLI[121,122]. They exhibited individual optics and

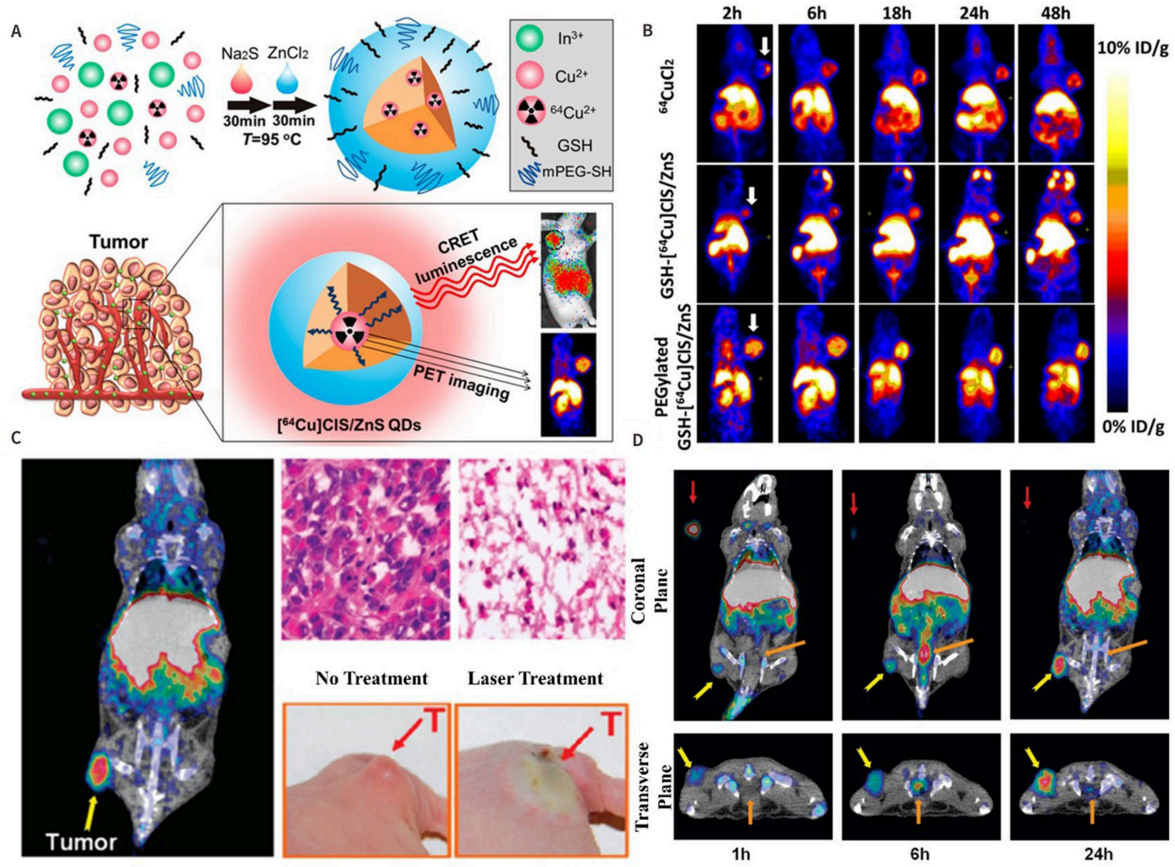

Figure 9. (A) Schematic synthesis of ^{64}Cu-CIS/ZnS QDs and PET imaging; (B)[119], (C), and (D) The micro-PET/CT imaging and tumor therapy *in vivo* ^{64}Cu-CuS nanoparticle[120]. (A)-(B): Copyright © *American Chemical Society* 2014; (C)-(D): Copyright © *American Chemical Society* 2010. CT: computed tomography; PET: positron emission tomography.

electronic characteristics. Additionally, their surface supports convenient coalition and ligand attachment[123-125].

In addition to their optical features, Cu nanoparticles also possess low toxicity and cost. Shi *et al.* developed a tumor-targeting and MMP2-activating nanoprobe by designing a novel magnetic semiconductor Gd/CuS nanoparticle named T-MAN. The researchers attested to its ability for FLI/MRI dual-modality imaging and precise PTT of gastric tumors[126]. Figure 10A showed the synthesis and structure of T-MAN, which involved micellar encapsulation of OA-coated Gd/CuS nanosheets assisted by amphiphilic DSPE-PEG. After intravenous injection, T-MAN can selectively enter into and characteristically accumulate in gastric tumors through active delivery mediated by αvβ3 integrin. Once accumulated in the gastric tumor tissue, it can be efficiently activated by αvβ3-bounded MMP-2; as a result, extracellular matrix-overexpressing MMP-2 produced significantly enhanced NIR fluorescence and strong T1-weighted MR Contrast imaging, which enabled accurate delineation of the gastric tumor. Under the guidance of fluorescence/MR dual-modality imaging, irradiation of gastric cancer tissue with 808 nm laser irradiation can produce high heat and eventually lead to irreversible tumor cell death, as demonstrated mathematically in Figure 10B. Figure 10C showed the schematic mechanism of *in vivo* PTT of gastric cancer guided by it using FLI/MRI dual-modality imaging, a schematic diagram of FLI/MRI biological model imaging and PTT of lymph node metastasis in live mice, T1-weighted MR images, and fluorescence images of metastatic and normal lymph

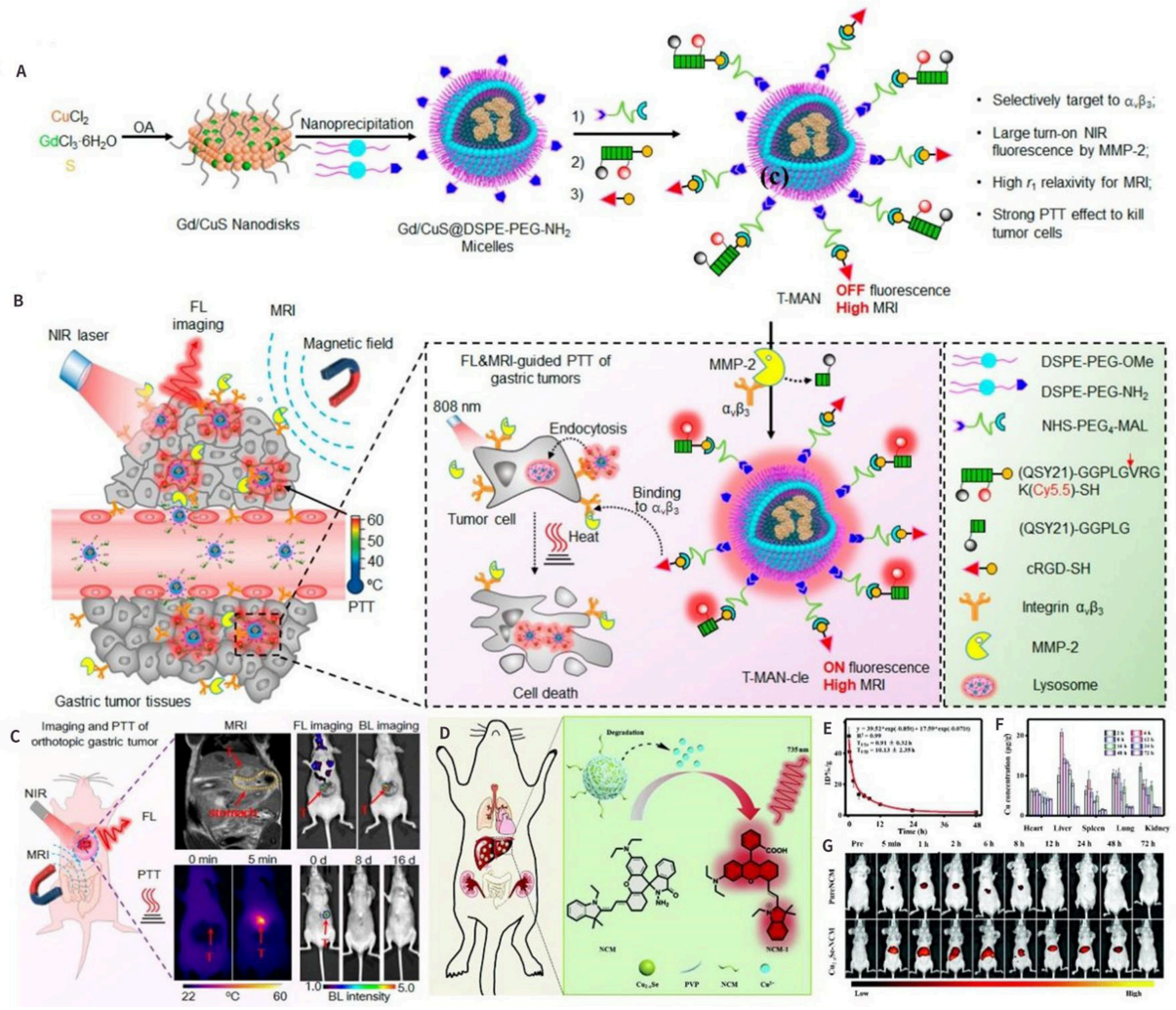

Figure 10. (A) and (B) General Design of T-MAN for Fluorescence/MR Bimodal Imaging and Targeted PTT of Tumors; and (C) schematic representation for fluorescence/MR imaging-guided PTT in gastric tumors *in vivo*[126]; (D)-(F) Illustration of fluorescence imaging by monitoring; and (G) the fluorescence images of ultrasmall $Cu_{2-x}Se$ nanoparticles[127]. (A)-(C): Copyright © *American Chemical Society* 2019; (D)-(G): Copyright © *The Royal Society of Chemistry* 2019. NIR: near-infrared region; MR: magnetic resonance; MRI: magnetic resonance imaging; PTT: photothermal therapy.

nodes in live mice. Shi *et al.* also reported on another novel fluorescent CuS nanoparticle (CuS-Cy5.5-RGD) capable of noninvasive multimodal imaging and targeted PTT of gastric cancer cells with intra-lymph node metastases. In addition, it allowed for rapid and noninvasive self-monitoring of PTT efficacy on metastatic sentinel lymph nodes in living mice[107]. In another paper, a NIR Cu^{2+} particular responsive probe (named NCM) was synthesized by Han *at el.*, as shown in Figure 10D. It loaded ultrasmall copper selenide nanoparticles on the surface to monitor the systematical release of copper ions in cells and animals[127]. Figure 10E and 10F show the metabolic and tissue distribution of the material. Meanwhile, the unlocked Cu^{2+} can react particularly with non-fluorescent NCM to form NCM-1 with strong NIR fluorescence to realize the FLI at 735 nm, as shown in Figure 10G. It consisted of cuprous selenide as the main body and was loaded with the non-fluorescent dye NCM. After the material was stimulated *in vitro* to release copper ions and activate dyes, FLI can be achieved and used for both *in vivo* and *in vitro* fluorescence imaging.

It is expected that the FLI in the visible spectroscopy and the NIR-I windows has some limitations and disadvantages[128-130], such as insufficient spatial resolution and penetration and a lack of anatomical structure information. This is due to the mutual effects between light and living tissues, which can cause rigorous autofluorescence, scattering, and absorption[131]. To overcome these problems, the range of FLI has been broadened to the NIR-II region[125].

Photoacoustic imaging

The material must have a strong photothermal conversion efficiency to be used in photoacoustic imaging (PAI). Because of their strong absorption of copper chalcogenides in the near-infrared region (700-1,500 nm), they have become the preferred choice for photothermal conversion agents[132]. The use of copper-based chalcogenides as photothermal reagents was first reported by Li *et al.* in 2000, who synthesized -SH-coated copper sulfide nanoparticles[133]. According to the existing reports, some copper chalcogenides X_2Y (X = Cu/Ag/Au, Y = S/Se/Te) were worthy of consideration because of their easy molecular formula, complicated crystal texture, and fickle composition, which provide inconceivably rich properties for a variety of applications of thermal conversion. Their characteristics in PAI and PTT have been owing to the strong LSPR absorption in the NIR window generated from copper deficiency[134]. Zhang *et al.* reported a novel application of ultra-small cuprous selenide as a photothermal therapeutic agent for multimodal imaging[135], which is shown in Figure 11A and B. It demonstrated the synthesis process of the material and its imaging and therapeutic applications *in vivo*. The $Cu_{2-x}Se$ had long circulation times in the blood and can accumulate at tumor sites through the enhanced permeability and retention effect. In addition, they can be labeled with nuclides (^{99m}Tc) for SPECT imaging to reveal tumor foci. Bao *et al.* developed a nanocomplex by modifying PD1 with gold nanoparticles on the surface of $Cu_{2-x}Se$ (GPSeCS@PD-1) and applied it to imaging and treating tumor-bearing mice. The PAI and PTT images in Figure 11C and D showed an obvious contrast between the PAI signal and the high temperature of 53.4 °C. This temperature caused the cancer cells to heat up and necrosis of cancer cells. PTT treatment has obvious inhibition and ablation effect. Bao *et al.* and other contributors have used synthetic copper for PAI and PTT[136]. The synthetic copper was widely used for PAI and PTT by Chen *et al.*[137] and other contributors[74,138,139].

Diagnosis and therapy of cancer

Cancer has become a significant threat to our well-being and health in modern society[140]. Currently, surgery, chemotherapy, and radiotherapy remain the primary strategies for cancer therapy. However, limited by indication, contraindication, and side effects of operation, chemotherapy and radiotherapy are usually reserved for patients with moderate or advanced cancer. To a certain extent, these treatments can cause additional pain and other toxic side effects for patients. In the field of senior nanoscience, single nanoparticles could afford diverse methods for diagnosis and therapy[74]. They are utilized by their physical and chemical properties of the nano-agents or through surface modification loading with different kinds of imaging and therapeutic agents[141]. Due to the enhanced permeability and retention[142,143] effect, they can be engineered to respond to precise stimuli, providing physicians with diagnostic and treatment response information. Endogenous stimuli, such as pH changes[144], hypoxia, and enzymes present in the tumor microenvironment (TME)[144-147], as the same as visually applied exogenous stimuli, including light[145], temperature, ultrasound, and magnetic field, are essential for the early cancer diagnosis and therapy.

An earlier diagnosis is essential for better medical outcomes and higher 5-year survival rates. Thus, one of the key-knob to precise cancer treatment is how to understand the targeting procedure. Up to now, there are several strategies to improve the NPs based targeting efficiency. For example, one common approach is to combine nanoparticles with folic acid (FA)[144], targeting peptides[147] or antibodies[130] to achieve receptor-mediated endocytosis, which has an instant effect on the enhancement of diagnostic value toward a wide diversity of cancers.

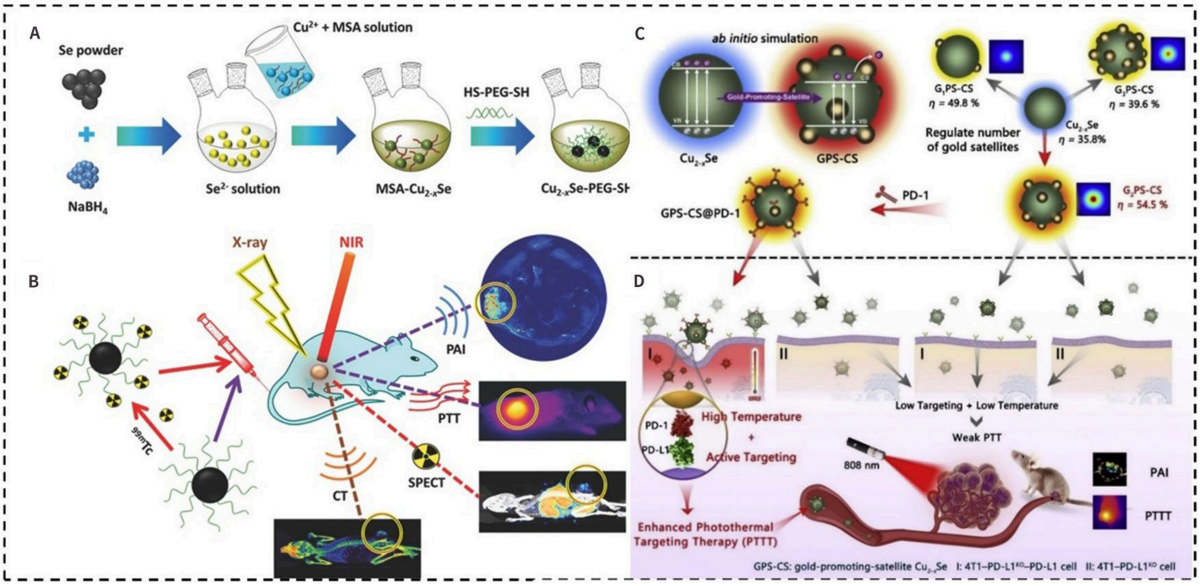

Figure 11. Schematic representation of the synthesis process of ultra-small $Cu_{2-x}Se$-PEG-SH; and (B) PA imaging, CT imaging, SPECT imaging, and photothermal therapy of cancer in vivo[135]; (C) Representative illustration of GPSeCS@PD-1 and the enhanced PTT (D) for triple-negative breast cancer[136]. (A)-(B): Copyright © *Wiley-VCH* 2016; (C)-(D): Copyright © *Elsevier Ltd.* 2022. CT: computed tomography; NIR: near-infrared region; PAI: photoacoustic imaging; PTT: photothermal therapy; SPECT: single-photon emission computed tomography.

Copper chalcogenides, as one of the potential agents, with aforesaid unique chemical, optical, and physical properties[105,148], have been widely used in tumor treatment fields such as PTT, PDT, CDT, and IT. However, the therapeutic efficacy largely depends on many factors, such as LSPR, particle size, laser wavelength, intensity, and the concentration of H_2O_2 within the tumor. Therefore, we address these factors in the reported literature and summarize the copper chalcogenides-based combination therapy to achieve the desired efficacy in Table 2, including PTT/chemotherapy, PDT/chemotherapy, CDT/chemotherapy, and chemotherapy/immunotherapy.

The application of each treatment modality will be briefly described next.

Photothermal therapy

PA imaging and Photothermal therapy (PTT) have been attributable to their LSPRs within the NIR window generated from copper deficiency[134]. The PTT technology is based on the nanoprobe with high photothermal conversion efficiency. Subsequently, the light irradiation with strong interaction with the designed copper chalcogenides probe, especially for the NIR light with deep penetration, most of the that would be turned into heat, resulting in the thermal ablation effect for the tumor. Thus, the combination of PTT and other strategies manifests high efficiency for tumor therapy and will be discussed in the following section.

Chemodynamic therapy

Chemodynamic therapy (CDT) is a burgeoning therapeutic method that takes advantage of Fenton-type reactions to go on highly toxic hydroxyl radicals (•OH) and other activated reactive oxygen species (ROS)[160-163]. It is known that the generation of •OH was generated by Fenton chemistry to depend on the relationship among the hydrogen peroxide (H_2O_2) and the catalyst and does not require oxygen (O_2) or external energy input. This individual mode of ROS generation allows CDT to overcome major barriers

Table 2. Comparison of the sizes, biological models, and bioapplications of nanoscale copper chalcogenides for cancer diagnosis and therapy

Materials	Size (nm)	Model	Bioapplications	Ref.
AM@DLMSN@CuS/R848	100	4T1	PTT/IT	[149]
Cu_9S_5@mSiO$_2$-PEG	45	Hep3B	PTT	[150]
Cu_{2-x}Se-PEG-SH	3.6	4T1	PAI/CT/SPECT/PTT	[135]
PEG-[^{64}Cu]CuS NPs	11.9	Hth83 ATC	PET/CT/+PTT/RT	[151]
CP Nanodots	16.3	U87MG	CDT	[152]
CuS NPs-PEG-Mal	12	4T1	IT	[153]
Cu_7S_4-Au@PSI-^{19}F/PEG	14	4T1	CT/^{19}FMRI/PTT	[105]
Cu_{2-x}Se-NCM	1.7	Raw	FLI	[127]
Gd/CuS@DSPE-PEG-MAL	56	MKN45	FLI/MRI/PTT	[126]
Cu_{2-x}Se/Bi_2Se_3@PEG	15	HepG2	CT/MRI/CDT/PDT/PTT	[106]
G5-PBA@CuS/cGAMP	3.6	B16-F10	PTT/IT	[154]
IR820@CuS/Pt JNMs	142	4T1	FLI/PTT/PDT	[155]
AuNBP@CuS	105	EMT-6	PTT/PDT/CDT	[156]
Lipo@ICG@CuS	145	4T1	FLI/PTT/PDT	[157]
Bac@Cu_2O	120	CT26	FLI/CDT	[158]
DOX/HCuS@PDA-MB	140	MDA-231	FLI/PTT/Chemotherapy	[159]

CDT: Chemodynamic therapy; CT: computed tomography; FLI: fluorescence imaging; ^{19}FMRI: fluorine-19 (^{19}F) magnetic resonance imaging; IT: Immunotherapy; MRI: magnetic resonance imaging; PAI: photoacoustic imaging; PET: positron emission tomography; PDT: photodynamic therapy; PTT: photothermal therapy; RT: radiation therapy; SPECT: single-photon emission computed tomography.

such as limited light penetration depth and hypoxia-related resistance in tumor PDT[152,164-168]. It was a ROS-mediated therapeutical method and utilized nano-catalytic medicine and the exogenetic stimulation to particularly convert H_2O_2 and O_2 into •OH and $^1O_2$ intra-tumor. As a result, cancer cells can be effectively and safely killed without harming normal tissues[118,166,169].

Recently, diverse metal-doped metallic peroxides (MPs), including metal ions and peroxo group (such as Fe, Mn, Cu, and Co) nanomaterials[170-172], have been developed as highly efficient nano-catalytic medicines to stimulate the generation of ROS because of their great peroxidase-like activity. Lin *et al.* reported on the manufacture of copper peroxide (CP) nanodots, which were the first samples to have Fenton- competence metal peroxide nanomaterials[152]. The CP nanodots were used as an activatable agent to enhance CDT through self-supplying H_2O_2, as shown in Figure 12A. In the picture, we could see that, after the internalization by cells, the CP was resolved in the acidic endo/lysosomal compartments because of the sensitivity to pH[152]. The anti-cancer chemo-dynamic effectiveness of CP nanodots was turned out both *in vitro* and *in vivo*. The specific strategies were shown in Figure 12A: there were lots of cases of chemo-dynamic therapy for copper chalcogenides nanoparticles from some researchers[149,173].

Wu *et al.* also confirmed that the Cu-based system is more efficient than conventional Fe-based Fenton agents in CDT[118]. A pH-responsive engineered covalent organic framework of CuS was designed in the tumor environment by Wang *et al.*, as shown in Figure 12B. Because of the regional excess temperature induced by PTT can further improve the CDT efficiency of the nano platform, which could lead to a synergistic PTT/chemotherapy/CDT effect[175]. Zuo *et al.* pioneered a credible paradigm to integrate photothermal and Fenton-like activities into one nanoplatform, as shown in Figure 12C[174]. It showed the synthesis procedure for CuS@COFs NPs and their application for CDT and PTT.

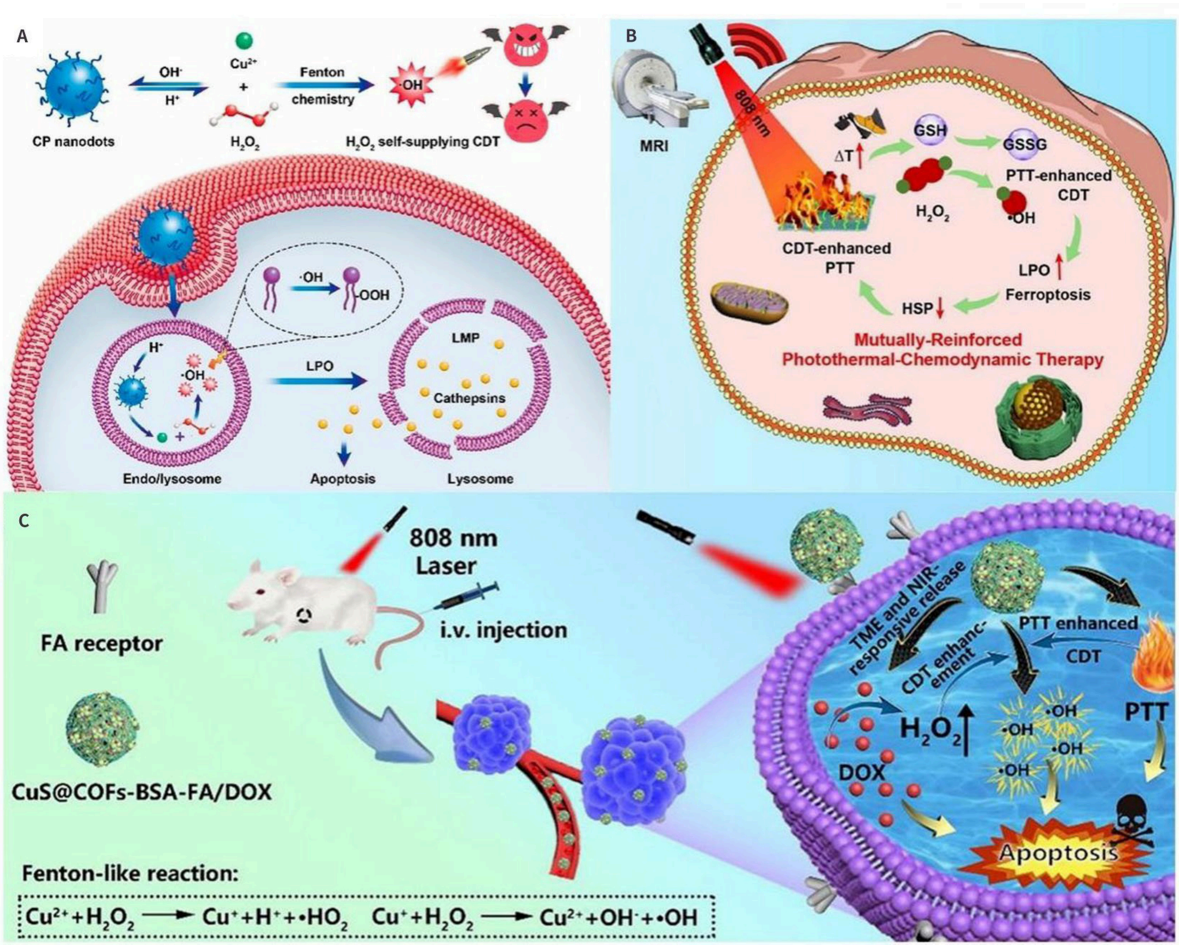

Figure 12. (A) Schematic representation of the synthesis of CP nanodots and their use of H_2O_2 self-supplying CDT[152], Copyright © *American Chemical Society* 2019; (B) Schematic representation of the synthesis process of CuCo NS and the therapeutic mechanism of mutually enhancing PTT-CDT[174], Copyright © *Elsevier B.V.* 2022; (C) Schematic illustration of CuS@COFs-BSA-FA/DOX preparation and the mechanisms of intracellular CDT action[175], Copyright © *Elsevier B.V.* 2022. CDT: chemodynamic therapy; CP: copper peroxide; FA: folic acid; HSP: heat shock protein; LPO: lipid peroxide; PTT: photothermal therapy.

Photodynamic therapy

The pattern of nanomaterials for photodynamic therapy (PDT) has attracted much attention regarding their therapeutic effects. Previous research demonstrated that CuS NCs modified with the progressive chlorine e6 (Ce6) named CuS-Ce6 processed capabilities as a multi-model agent for PTT and PDT[176]. Under the 670 nm laser irradiation, CuS-Ce6 showed high PDT effects through singlet oxygen generation and thermal ablation with 808 nm laser irradiation, as shown[177] in Figure 13A. In a separate report, Han *et al.* showed that the cavitated CuS nanoparticles, modified with bovine serum albumin (BSA) and folic acid complex and loaded with ICG, named CuS-BSA-FA, as shown in Figure 13B. PDT and PTT were combined to provide a conjunct therapy that exhibited a perfect PTT heating effect, generation of $^1O_2$, and laser irradiation significantly effective compared to other nanocarriers[178]. Liu *et al.* proposed DSF-loaded hollow CuS nanoparticles named DSF@PEG-HCuSNPs with the NIR-II region induced and the PTT effect enhanced. The DSF-initiated cancer chemotherapy had been explored as a means to achieve TME that could activate the formation of cytotoxic $Cu(DTC)_2$ *in situ*[179]; this was shown in Figure 13C, where Cu^{2+} and DSF drug molecules could be rapidly released and degraded in an acidic microenvironment with high PTT-conversion efficiency (23.8 %) near the NIR-II bio-window. Chen *et al.* successfully developed a

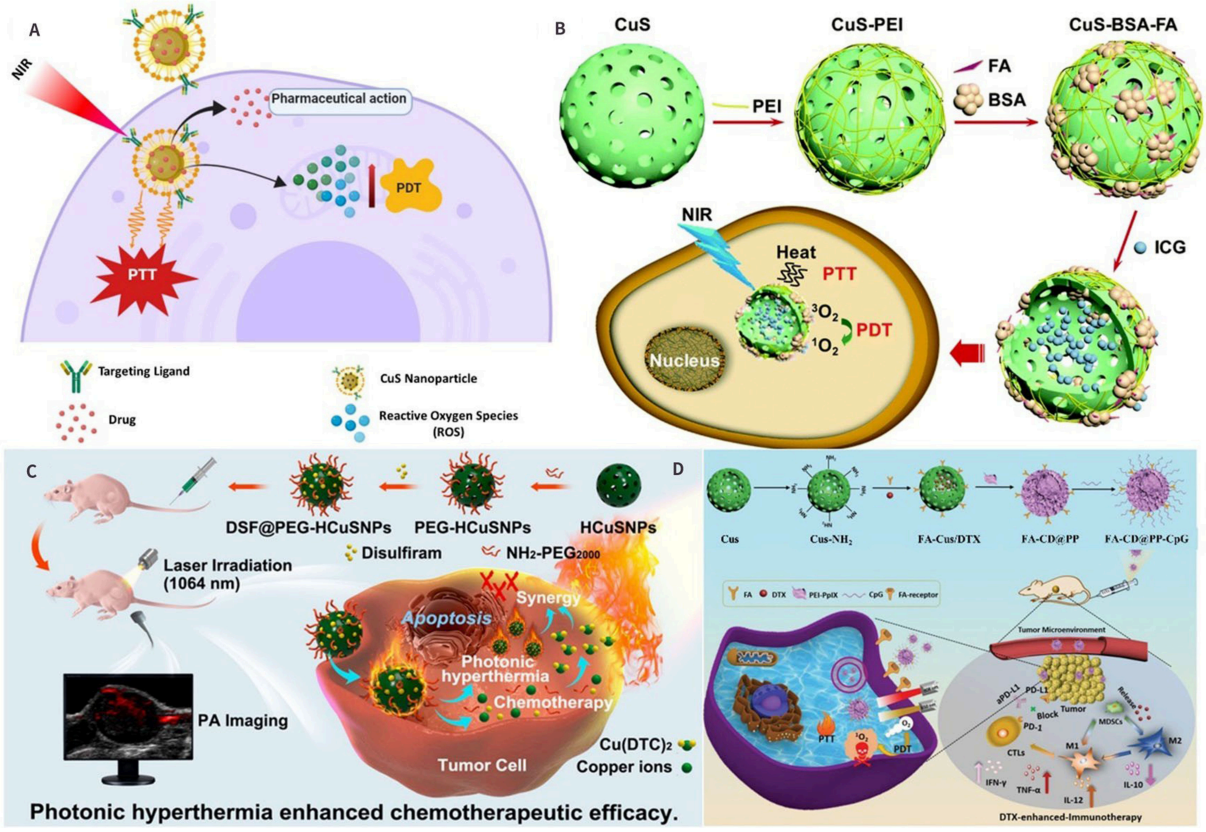

Figure 13. (A) The schematic diagram of multimodal diagnosis and treatment of CuS NPs[177], Copyright © *Elsevier B.V.* 2020; (B)The schematic representation of the role of CuS-BSA-FA in PDT and PTT[178], Copyright © *Royal Society of Chemisrty* 2012; (C) Schematic representation of the preparation of DSF@PEG-HCuSNPs (top) and the corresponding synergistic effects of NIR-II-induced photonic hyperthermia and in situ formation of $Cu(DTC)_2$ complexes for enhancing the chemotherapeutic efficacy of DSF-based chemotherapy[179], Copyright © *American Chemical Society* 2021; (D) The rational design and synthesis of FA-CD@PP-CpG nanocomposites (top), their use in cancer therapy (left), and illustrations of FA-CD@PP-CpG for docetaxel enhanced immunotherapy (right)[180]; Copyright © *Wiley-VCH Verlag GmbH & Co. KGaA, Weinheim* 2019. BSA: bovine serum albumin ; FA: folic acid; ICG: indocyanine green; NIR: near-infrared region; PDT: photodynamic therapy; PEI: polyethyleneimine; PTT: photothermal therapy.

multifunctional FA-CD@PP-CpG for synergistic phototherapy (including PDT and PTT) and docetaxel-enhanced immunotherapy. They exhibited excellent PDT efficiency and PTT-conversion capability under 650 nm and 808 nm irradiation, as shown in Figure 13D. What is more, they were able to significantly inhibit tumor growth of 4T1-bearing mice *in vivo* without significant side effects. Low-dose docetaxel loading can promote permeability, improve the effectiveness of anti-PD-L1 antibody (aPD-L1), inhibit MDSCs, reduce tumor burden, effectively polarize MDSCs to M1 phenotype, and further enhance anti-tumor efficacy. In summary, the nanocomposites mentioned above provide an effective synergistic therapeutic modality for cancer[180].

Radiation therapy

Radiation therapy (RT) was utilized as a therapeutic strategy to attract cell death in the target sites by causing precise DNA damage. RT can be implemented using various techniques, including external beams such as electrons, protons, and brachytherapy[181-183]. Many β-emitting NPs have been proposed as reasonable agents for cancer RT.

As depicted in Figure 14A, the latest trials involving the combination of Cu chalcogenides-based multimodality were discussed[184]. In the following, we will briefly describe methods to further improve this collaborative therapy, such as achieving image-guided collaborative therapy, promoting penetration into the deep part of the tumor, and enhancing ROS induced in the TME. Zhou *et al.* reported a $Cu_{2-x}Se$@PtSe (CSP) nano-sensitizer that resembled a yolk-shell structure was enhanced by the HIF-1α inhibitor acriflavine (ACF), as shown in Figure 14B. It alleviated tumor hypoxia and blocked the G2/M phase to enhance the radiosensitivity; moreover, it exhibited strong X-ray attenuation due to its high-Z element composition, thereby enhancing the radiotherapy effect on the mouse breast cancer model[185]. It demonstrated the excellent potential of the resultant functional nano-sensitizers of tumor radiotherapy. Peng *et al.* prepared the high-Z element-based hollow mesoporous TaOx nanospheres with the following growth of ultrasmall CuS nanocrystals. Then they packaged with O^{2-} saturated perfluoropentane (PFP), named HMTCP@PFP@O_2[186]. It exhibited prominent PTT efficiency, well biocompatibility, the ability to concentrate the energy of irradiation, and the capacity to carry strong oxygen. Therefore, it can be used for tumor RT, as shown in Figure 14C. A spindle-shaped CuS@CeO_2 core-shell nanoparticles were synthesized by Jiang *et al.*, which simultaneously combined self-oxygen supply, photothermal ability, and radiosensitization, as shown in Figure 14D[187]. CeO_2-encapsulated CuS nanoparticles can be stably released and penetrate deep into the tumor, thereby reducing the effect of radiotherapy on lesion regression. Moreover, it has shown that the design not only reduces the radiotherapy dose but, more importantly, treats the entire tumor without recurrence.

Immunotherapy

The diagnosis and therapy of cancer have been extensively discussed in the previous literature. One of the main reasons for the failure of cancer treatment is tumor metastasis and recurrence. Immunotherapy, the Nobel Prize in Physiology or Medicine of 2018, has brought hope and opportunity to address this issue.

Immunogenic cell death (ICD) was more likely to be induced by deep tumor penetrating ablation, resulting in a more uniform distribution of released tumor antigens[189]. Tumor PTT, as mentioned above, has attracted more attention due to its advantages of low adverse reactions and non-invasiveness for cancer treatment. However, the hyperthermia therapy strategy alone is still inadequate to inhibit tumor metastasis and recurrence. Therefore, the combination strategy with *Immunotherapy (IT)* presents significant therapeutic efficiency for malignant tumors, which opens a new avenue for cancer therapy.

Wang *et al.* developed a surface-functionalized CuS NP named CuS-PEG-Mal[153], which can be used not only for tumor hyperthermia as photothermal media but also as an antigen-capture agent to adsorb tumor antigens released during hyperpyrexia to induce anti-tumor immune responses. As shown in Figure 15A, an immune checkpoint inhibitor was combined with anti-PD-L1 to evaluate the efficacy of CuS-mediated hyperthermia in improving tumor immunotherapy through surface-functionalized modification. Yan *et al.* reported a collaborative photothermal immunotherapy device for Cas9 riboprotein targeting PTPN2 based on the CuS nanotherapeutic platform[188]. HS-modified DNA (DNA-SH) chippings were coupled with CuS and combined with Cas9 RNP via base complementary pairing methods. They are then coated with endosomal destructive polyethyleneimine (PEI), as shown in Figure 15B, and named CuS-RNP@PEI (CRP). It was endocytosed by cancer cells because of the modification of the cationic PEI on the surface of NPs. After PEI-assisted endosomal escape, CRP was released into the cytoplasm and improved by photothermal induction of double-strand breaks provided by NIR-triggered CuS, as shown in Figure 15C. Thus, this NIR light-triggered therapy platform provides a multifunctional therapeutic strategy with a synergetic effect, namely, "1 + 1 > 2". What is more, for the combination of multimodal therapies described above, one of the main challenges is developing an appropriate vector institution for efficient co-loading and targeted delivery

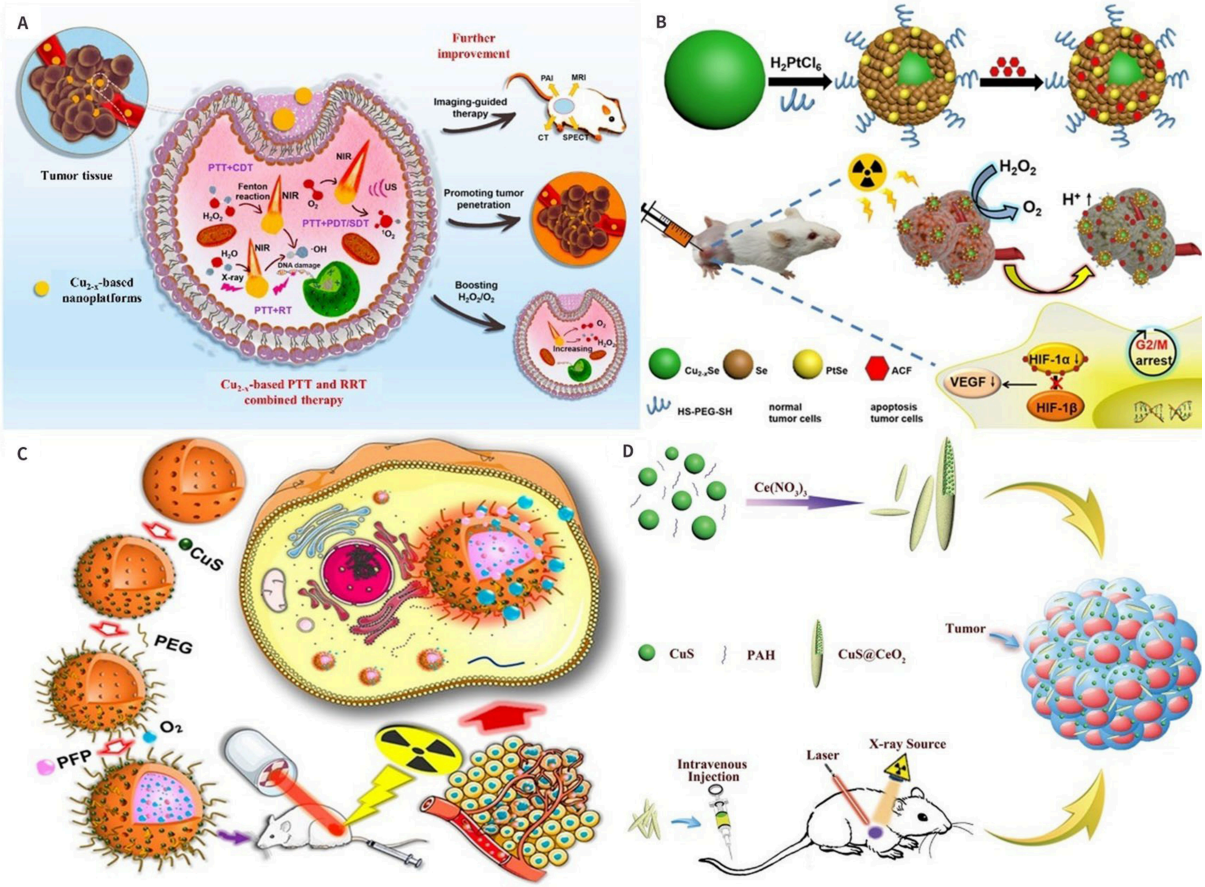

Figure 14. (A) Schematic illustration of Cu_{2-x}E-based PTT and RRT[184], Copyright © *American Chemical Society* 2020; (B) Synthesis of CSP-ACF nanoparticles and mechanism of CSP-ACF nanoparticles combined with X-rays in killing 4T1 tumors[185], Copyright © *American Chemical Society* 2020; (C) The therapeutic functions of HMTCP@PFP@O_2 enhance radiosensitization in vivo[186], Copyright © *American Chemical Society* 2020; (D) Schematic representation of the synthesis of nanomaterials and their mechanisms of action in radiotherapy[187], Copyright © *Wiley-VCH Verlag GmbH & Co. KGaA* 2019. ACF: acriflavine; CSP: Cu_{2-x}Se@PtSe; CDT: chemodynamic therapy; NIR: near-infrared region; PFP: perfluoropentane; RT: Radiation therapy; RRT: ROS-related therapy; VEGF: vascular endothelial growth factor.

of checkpoint inhibitors, immune adjuvants, and CuS NPs. As shown in Figure 15D, an intelligent bio-inspired nanoplatform based on dendritic large pore mesoporous silica nanoparticles (DLMSNs), named AM@DLMSN@CuS/R848, was designed by Cheng *et al.*[149]. Both CuS NPs with high PTT-conversion efficiency and immune adjuvant (R848) were artfully embedded inside the macropores of DLMSNs, as shown in Figure 15E, and were utilized for the depression of metastatic tumors.

Although the achievement of immunotherapy is sensational, its clinical applications were still inhibited by the immunosuppressive environment in the tumor. Immunotherapy approaches are often ineffective due to the highly complex immune suppression mechanisms in the TME and subjective deviations in patient reactions. Therefore, combining multiple immune activation mechanisms is considered to be the best strategy for tumor treatment. Among them, immunogenicity and/or immune-related adverse effects from antibody preparations, such as skin, gastrointestinal tract side effects, pneumonia, and hepatitis, were other challenges for the widespread clinical application of cancer IT. Therefore, there is an urgent requirement to identify effective synergetic strategies to improve the therapeutic efficacy while mitigating the systemic

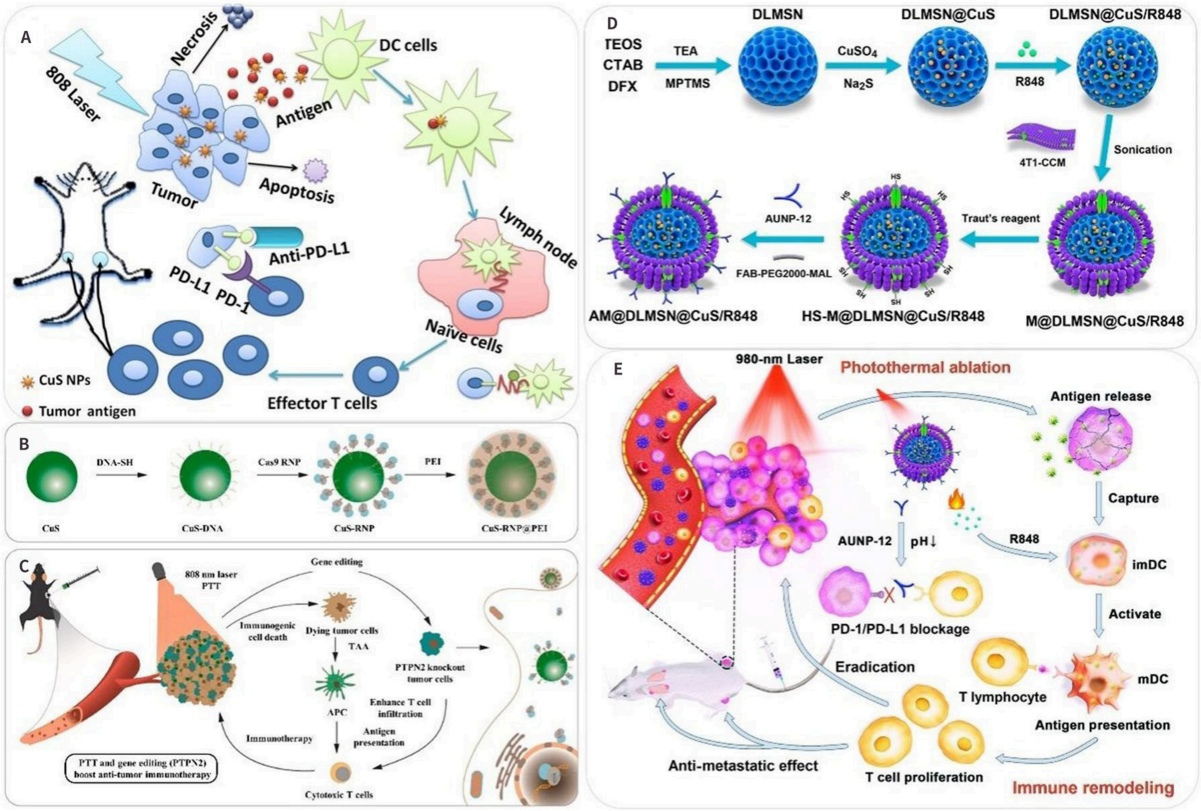

Figure 15. Example of the application of copper chalcogenide nanoparticles in animal immunotherapy. (A) Schematic of anti-tumor immune responses induced by CuS-PEG-Mal-based PTT plus immune checkpoint inhibitors[153]; (B) Illustration of gradually synthesized CuS-RNP@PEI; and (C) Copper-based NIR photo-triggered synergetic photothermal cancer immunotherapy vectors and PTPN2 targeted immunotherapy[188]; (D) Schematic diagram of preparation and synthesis of AM@DLMSN@CuS/R848; (E) AM@DLMSN@CuS/R848 has a synergistic therapeutic effect on triple-negative breast cancer TNBC by combining photothermal ablation and immune remodeling[149]. (A): Copyright © *American Chemical Society* 2019; (B)-(C): Copyright © *Elsevier Ltd.* 2021; (D)-(E): Copyright © *American Chemical Society* 2020. PEI: polyethyleneimine; PTT: photothermal therapy.

toxicity of cancer immunotherapy.

Synergetic therapy

A combination of multitudinous treatments has a synergistic effect on various real tumors, resulting in significantly enhanced therapy effectiveness. Many nanomaterials have a large precise superficial area and can be used as an available carrier for some drugs and agents. There are a lot of reports about the coating of silica on PTT reagents, enabling the combination of multitudinous treatments for cancer[74,150]. Therefore, it is expected that the CuS@mSiO$_2$ not only possesses high biocompatibility[150] but also has the potential to be a multifunctional platform for effective PTT, chemotherapy, and infrared thermal imagining applications, as shown in Figure 16A and B. In another study by Guo *et al.*[138], they combined ultrasonic detection with optical excitation, which can overcome the limits of penetration depth more than traditional optical imaging technology. They also lead an imaging-guided synergistic tumor therapy with rapid excretion properties, as shown in Figure 16C. Before the bio-experiment, Figure 16D and E showed the biosafety of the CFPP NPs. They demonstrated enhanced PTT efficiency due to the LSPR absorption (1,064 nm) in the second near-infrared (NIR-II) region, apart from the assembly and light penetration depth, as shown in PAI/MRI/PTI in Figure 16F-J. Zhou *et al.* conducted a study to enhance the therapeutic efficacy of RT combined with PTT in tumors, and the anti-tumor experiments showed that tumor growth was effectively

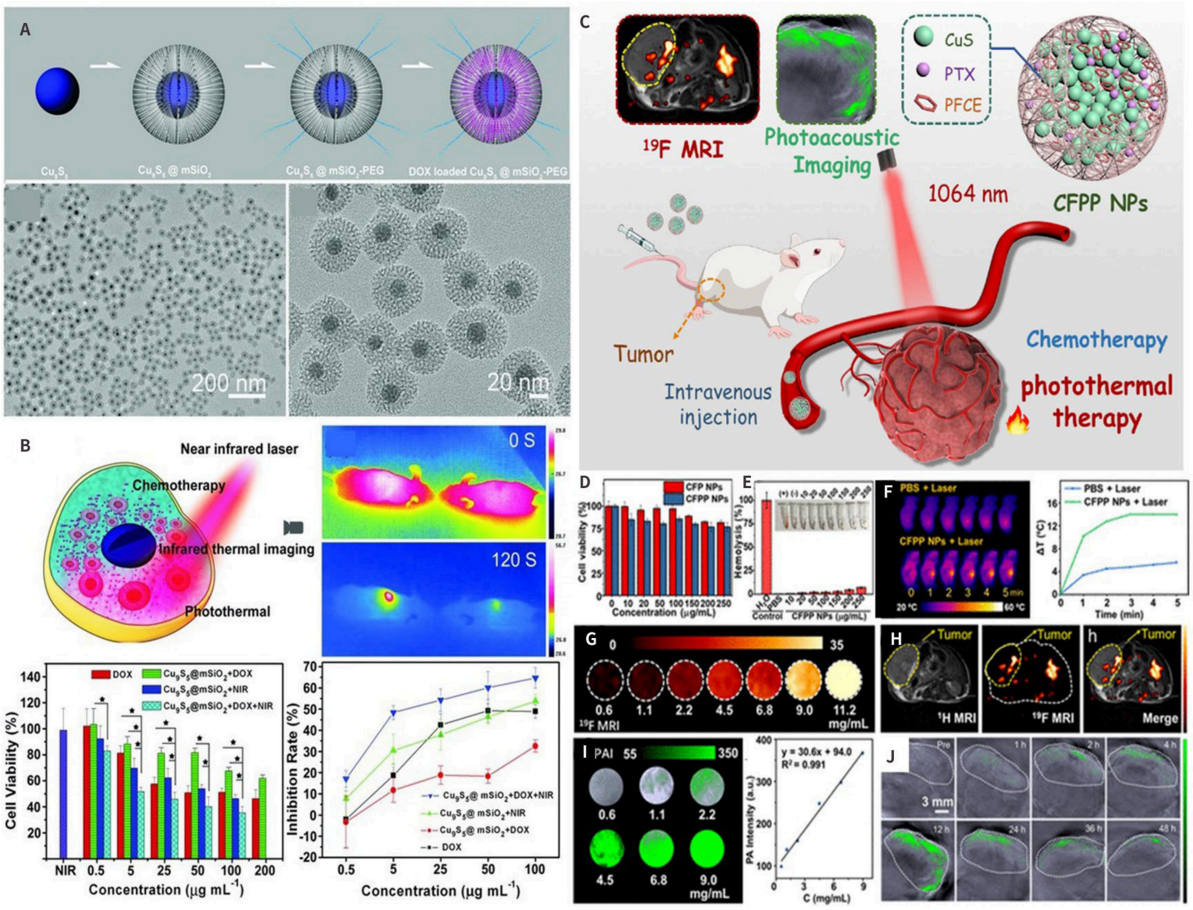

Figure 16. Photothermal enhanced chemotherapy: (A) The synthetic protocol of the Cu_9S_5@$mSiO_2$-PEG[150]; (B) Illustration of the tumor-specific in situ transition chelating reaction and augmentation generated by photothermal effect under NIR laser irradiation; (C) Chemo-photothermal synergistic therapy: Schematic Illustration of Fabrication and Bioapplication of CFPP NPs and (D) and (E) Photothermal images (F) PAI of CFPP NPs at different times after intravenous injection; (G) MRI of CFPP NPs. (H) MRI in vivo (I) PAI of CFPP NPs at different concertation of CFPP and (J) PAI *in vivo*[138]. (A)-(B): Copyright © *Wiley-VCH* 2013; (C)-(J): Copyright © *American Chemical Society* 2022. MRI: magnetic resonance imaging; PAI: photoacoustic imaging.

delayed by the combination of RT/PTT[151].

CONCLUSION AND OUTLOOK

This review briefly concluded the structure and synthesis strategy for copper chalcogenide compounds. In addition, the theoretical method for the plasmonic copper-based doped NCs is discussed. And we also present the wildly reported heavy doping strategies for the formation of plasmonic colloidal copper chalcogenides NCs, including (1) electronic doping; (2) photo doping; (3) morphology, and surface ligands effects; and (4) hybrid structure. As discussed above, the LSPR feature was determined by the free carrier density. On the one hand, we can tune the distribution of carriers (including their shapes, sizes, and surface properties); on the other hand, we can manipulate the density of the free charge carriers (such as light or electrochemical doping strategy). Finally, we introduce devious applications, including bioimaging, cancer therapy, and biosensing. Although the formation of the heavily-doped copper chalcogenides with LSPR feature has already attracted significant attention due to their various potential applications, the development of the plasmonic copper chalcogenides for the next generation should also be taken into consideration.

The toxicity and safety of nano-copper chalcogenide compounds are of primary concern, which is an important issue for their biological applications. Unfortunately, few systematic studies have investigated the toxicity and biological results caused by recycling, biodistribution, degradation, and metabolism of Cu sulfide NCs after drug administration. The majority of studies have been devoted to their efforts on the viability of various cell species. We sum up with original expectations and propose future directions for the clinical application of these novel schemes for synergistic therapy.

Advanced imaging modalities and tumor treatment modalities based on copper sulfur compounds provide a possibility for clinical diagnosis, treatment, and basic research. At the same time, the biotoxicity of Cu chalcogenides is greatly reduced after surface modification, which provides a broad prospect for their practical applications. Compared with the development of ferroptosis, cuproptosis has been presented as an effective therapeutic strategy for cancer treatment[190,191]. However, the precise mechanism for Cu apoptosis and its related signaling pathways are still unclear.

Further, the large-scale synthesis strategy for industrialization and clinic is worth considering. The transformation from lab-made to everyday use is essential for the potential application.

Overall, the development of plasmonic copper chalcogenides is promising, especially for biological applications. In my opinion, the emergence of the "new copper generation" is just around the corner.

DECLARATIONS

Authors' contributions

Wrote the manuscript: Mao Q, Ma J
Revised the manuscript: Mao Q, Ma J, Chen M, Lin S, Razzaq N
Guided this work and rewrote parts of the manuscript: Cui J
Mao Q and Ma J contributed equally to this work.

Availability of data and materials

Not applicable.

Financial support and sponsorship

This work was supported by the National Natural Science Foundation of China (No. 22104105), the Natural Science Foundation of Jiangsu Province (No. BK20210702), Leading Talents of Innovation and Entrepreneurship of Gusu (No. ZXL2022515), and Research Fund from Soochow University (No. NH12800122).

Conflicts of interest

All authors declared that there are no conflicts of interest.

Ethical approval and consent to participate

Not applicable.

Consent for publication

Not applicable.

REFERENCES

1. Panfil YE, Oded M, Banin U. Colloidal quantum nanostructures: emerging materials for display applications. *Angew Chem Int Ed Engl* 2018;57:4274-95. DOI PubMed PMC
2. Saldanha PL, Lesnyak V, Manna L. Large scale syntheses of colloidal nanomaterials. *Nano Today* 2017;12:46-63. DOI
3. Shim M, Guyot-Sionnest P. n-type colloidal semiconductor nanocrystals. *Nature* 2000;407:981-3. DOI PubMed
4. Carulli F, Pinchetti V, Zaffalon ML, et al. Optical and magneto-optical properties of donor-bound excitons in vacancy-engineered colloidal nanocrystals. *Nano Lett* 2021;21:6211-9. DOI PubMed PMC
5. Hartley CL, Kessler ML, Dempsey JL. Molecular-level insight into semiconductor nanocrystal surfaces. *J Am Chem Soc* 2021;143:1251-66. DOI PubMed
6. Roth AN, Chen Y, Adamson MAS, et al. Alkaline-earth chalcogenide nanocrystals: solution-phase synthesis, surface chemistry, and stability. *ACS Nano* 2022;16:12024-35. DOI
7. Granados Del Águila A, Liu S, Do TTH, et al. Linearly polarized luminescence of atomically thin MoS_2 semiconductor nanocrystals. *ACS Nano* 2019;13:13006-14. DOI PubMed
8. Camats M, Pla D, Gómez M. Copper nanocatalysts applied in coupling reactions: a mechanistic insight. *Nanoscale* 2021;13:18817-38. DOI PubMed
9. Pellei M, Del Bello F, Porchia M, Santini C. Zinc coordination complexes as anticancer agents. *Coord Chem Rev* 2021;445:214088. DOI
10. Chábera P, Liu Y, Prakash O, et al. A low-spin Fe(iii) complex with 100-ps ligand-to-metal charge transfer photoluminescence. *Nature* 2017;543:695-9. DOI
11. Hu Z, O'Neill R, Lesyuk R, Klinke C. Colloidal two-dimensional metal chalcogenides: realization and application of the structural anisotropy. *Acc Chem Res* 2021;54:3792-803. DOI PubMed
12. Zhang J, Wang L, Chen F, Tang A, Teng F. Optical properties of multinary copper chalcogenide semiconductor nanocrystals and their applications in electroluminescent devices. *Chin Sci Bull* 2021;66:2162-78. DOI
13. Kim JY, Yang J, Yu JH, et al. Highly efficient copper-indium-selenide quantum dot solar cells: suppression of carrier recombination by controlled ZnS overlayers. *ACS Nano* 2015;9:11286-95. DOI PubMed
14. Yang W, Duan HS, Cha KC, et al. Molecular solution approach to synthesize electronic quality Cu_2ZnSnS_4 thin films. *J Am Chem Soc* 2013;135:6915-20. DOI PubMed
15. Just J, Coughlan C, Singh S, et al. Insights into nucleation and growth of colloidal quaternary nanocrystals by multimodal X-ray analysis. *ACS Nano* 2021;15:6439-47. DOI PubMed PMC
16. Lee JM, Kraynak LA, Prieto AL. A directed route to colloidal nanoparticle synthesis of the copper selenophosphate Cu_3PSe_4. *Angew Chem Int Ed Engl* 2020;59:3038-42. DOI
17. Mcclary SA, Balow RB, Agrawal R. Role of annealing atmosphere on the crystal structure and composition of tetrahedrite-tennantite alloy nanoparticles. *J Mater Chem C* 2018;6:10538-46. DOI
18. Agrawal A, Cho SH, Zandi O, Ghosh S, Johns RW, Milliron DJ. Localized surface plasmon resonance in semiconductor nanocrystals. *Chem Rev* 2018;118:3121-207. DOI PubMed
19. Wang J, Singh A, Liu P, et al. Colloidal synthesis of Cu_2SnSe_3 tetrapod nanocrystals. *J Am Chem Soc* 2013;135:7835-8. DOI PubMed
20. Liu G, Qi S, Chen J, Lou Y, Zhao Y, Burda C. Cu-Sb-S ternary semiconductor nanoparticle plasmonics. *Nano Lett* 2021;21:2610-7. DOI PubMed
21. Sun M, Fu X, Chen K, Wang H. Dual-plasmonic gold@copper sulfide core-shell nanoparticles: phase-selective synthesis and multimodal photothermal and photocatalytic behaviors. *ACS Appl Mater Interfaces* 2020;12:46146-61. DOI PubMed
22. Liu Z, Zhong Y, Shafei I, et al. Tuning infrared plasmon resonances in doped metal-oxide nanocrystals through cation-exchange reactions. *Nat Commun* 2019;10:1394. DOI PubMed PMC
23. Ali MA, Yuehui X, Liu X, Qiu J. Self-confined precipitation of ultrasmall plasmonic $Cu_{2-x}Se$ particles in transparent solid medium. *J Phys Chem C* 2019;123:9394-9. DOI
24. Liu Y, Liu M, Swihart MT. Plasmonic copper sulfide-based materials: a brief introduction to their synthesis, doping, alloying, and applications. *J Phys Chem C* 2017;121:13435-47. DOI
25. Arumugam GM, Karunakaran SK, Galian RE, Pérez-Prieto J. Recent Progress in lanthanide-doped inorganic perovskite nanocrystals and nanoheterostructures: a future vision of bioimaging. *Nanomaterials* 2022;12:2130. DOI PubMed PMC
26. Yang R, Mei L, Zhang Q, et al. High-yield production of mono- or few-layer transition metal dichalcogenide nanosheets by an electrochemical lithium ion intercalation-based exfoliation method. *Nat Protoc* 2022;17:358-77. DOI PubMed
27. Sreejith S, Huong TTM, Borah P, Zhao Y. Organic–inorganic nanohybrids for fluorescence, photoacoustic and Raman bioimaging. *Sci Bull* 2015;60:665-78. DOI
28. Ye K, Tang T, Liang Z, Ji H, Lin Z, Yang S. Recent progress of bismuth vanadate-based photoelectrocatalytic water splitting. *Chin Sci Bull* 2022;67:2115-25. DOI
29. Ge H, Kuwahara Y, Yamashita H. Development of defective molybdenum oxides for photocatalysis, thermal catalysis, and photothermal catalysis. *Chem Commun* 2022;58:8466-79. DOI PubMed
30. Chakraborty S, Mannar S, Viswanatha R. Local surface plasmon-assisted metal oxide perovskite heterostructure for small light emitters. *J Phys Chem C* 2021;125:10565-71. DOI

31. Staller CM, Gibbs SL, Saez Cabezas CA, Milliron DJ. Quantitative analysis of extinction coefficients of Tin-doped indium oxide nanocrystal ensembles. *Nano Lett* 2019;19:8149-54. DOI PubMed
32. Tandon B, Agrawal A, Heo S, Milliron DJ. Competition between depletion effects and coupling in the plasmon modulation of doped metal oxide nanocrystals. *Nano Lett* 2019;19:2012-9. DOI PubMed
33. Zandi O, Agrawal A, Shearer AB, et al. Impacts of surface depletion on the plasmonic properties of doped semiconductor nanocrystals. *Nat Mater* 2018;17:710-7. DOI
34. Zheng JW, Lebedev K, Wu SO, et al. High loading of transition metal single atoms on chalcogenide catalysts. *J Am Chem Soc* 2021;143:7979-90.10.1021/jacs.1c01097. DOI
35. Li XP, Huang RJ, Chen C, Li T, Gao YJ. Simultaneous conduction and valence band regulation of indium-based quantum dots for efficient H_2 photogeneration. *Nanomaterials* 2021;11:1115. DOI PubMed PMC
36. Liu X, Swihart MT. Heavily-doped colloidal semiconductor and metal oxide nanocrystals: an emerging new class of plasmonic nanomaterials. *Chem Soc Rev* 2014;43:3908-20. DOI PubMed
37. Zimmer D, Ruiz-fuertes J, Morgenroth W, et al. Pressure-induced changes of the structure and properties of monoclinic α -chalcocite Cu_2S. *Phys Rev B* 2018:97. DOI
38. Barman SK, Huda MN. Stability enhancement of Cu_2S against Cu vacancy formation by Ag alloying. *J Phys Condens Matter* 2018;30:165701. DOI PubMed
39. Zimmer D, Ruiz-fuertes J, Bayarjargal L, et al. Phase transition of tetragonal copper sulfide Cu_2S at low temperatures. *Phys Rev B* 2017:96. DOI
40. Khatri P, Huda MN. Prediction of a new phase of Cu*x*S near stoichiometric composition. *Int J Photoenergy* 2015;2015:1-7. DOI
41. Saona LA, Campo-Giraldo JL, Anziani-Ostuni G, et al. Cysteine-mediated green synthesis of copper sulphide nanoparticles: biocompatibility studies and characterization as counter electrodes. *Nanomaterials* 2022;12:3194. DOI PubMed PMC
42. Wang J, Zhuo K, Gao J, Landman U, Chou M. Mechanism for anisotropic diffusion of liquid-like Cu atoms in hexagonal β-Cu_2S. *Phys Rev Materials* 2021:5. DOI
43. Muddassir Y, Tahir S, Ali A, et al. Morphology-dependent thermoelectric properties of mixed phases of copper sulfide ($Cu_{2-x}S$) nanostructures synthesized by hydrothermal method. *Appl Phys A* 2021:127. DOI
44. Iqbal S, Bahadur A, Anwer S, et al. Effect of temperature and reaction time on the morphology of l-cysteine surface capped chalcocite (Cu_2S) snowflakes dendrites nanoleaves and photodegradation study of methyl orange dye under visible light. *Colloids Surf A Physicochem Eng Asp* 2020;601:124984. DOI
45. Asadov YG, Aliyev YI, Dashdemirov AO, Jabarov SH, Naghiyev TG. High-temperature X-ray diffraction study of Ag_2S-Cu_2S system. *Mod Phys Lett B* 2020;34:2150018. DOI
46. Maskaeva LN, Glukhova IA, Markov VF, Tulenin SS, Voronin VI. Nanostructured copper(I) sulfide films: Synthesis, composition, morphology, and structure. *Russ J Appl Chem* 2016;89:1939-47. DOI
47. Yarur Villanueva F, Green PB, Qiu C, et al. Binary $Cu_{2-x}S$ templates direct the formation of quaternary Cu_2ZnSnS_4 (Kesterite, Wurtzite) Nanocrystals. *ACS Nano* 2021;15:18085-99. DOI PubMed
48. Zhu D, Ye H, Liu Z, et al. Seed-mediated growth of heterostructured $Cu_{1.94}S$-MS (M = Zn, Cd, Mn) and alloyed $CuNS_2$ (N = In, Ga) nanocrystals for use in structure- and composition-dependent photocatalytic hydrogen evolution. *Nanoscale* 2020;12:6111-20. DOI
49. Liu W, Shi X, Gao H, et al. Kinetic condition driven phase and vacancy enhancing thermoelectric performance of low-cost and eco-friendly $Cu_{2-x}S$. *J Mater Chem C* 2019;7:5366-73. DOI
50. Chen L, Hu H, Chen R, Li Y, Li G. One-pot synthesis of roxbyite $Cu_{1.81}S$ triangular nanoplates relevant to plasmonic sensor. *Mater Today Commun* 2019;18:136-9. DOI
51. Yamamoto K, Kashida S. X-ray study of the cation distribution in Cu_2Se, $Cu_{1.8}Se$ and $Cu_{1.8}S$; analysis by the maximum entropy method. *Solid State Ion* 1991;48:241-8. DOI
52. Villa A, Telkhozhayeva M, Marangi F, et al. Optical Properties and Ultrafast Near-Infrared Localized Surface Plasmon Dynamics in Naturally p-Type Digenite Films. *Adv Opt Mater* 2023;11:2201488. DOI
53. Zhang Y, Feng J, Ge Z. Enhanced thermoelectric performance of $Cu_{1.8}S$ via lattice softening. *J Chem Eng* 2022;428:131153. DOI
54. Zhang Y, Xing C, Liu Y, et al. Doping-mediated stabilization of copper vacancies to promote thermoelectric properties of $Cu_{2-x}S$. *Nano Energy* 2021;85:105991. DOI
55. Kuterbekov K, Balapanov M, Kubenova M, et al. Thermal properties of nanocrystalline copper sulfides $K_xCu_{1.85}S$ ($0 < x < 0.05$). *Lett Mater* 2022;12:191-6. DOI
56. Janickis V, Petrasauskiene N. Modification of polyamide films by semiconductive and conductive copper selenide-copper sulfide layers. Available from: http://mokslozurnalai.lmaleidykla.lt/publ/0235-7216/2017/4/214%E2%80%93225pdf.pdf. [Last accessed on 11 May 2023]. DOI
57. Li Cheng, Li D, Yu W, et al. A novel strategy to fabricate CuS, $Cu_{7.2}S_4$, and $Cu_{2-x}Se$ nanofibers via inheriting the morphology of electrospun CuO nanofibers. *Russ J Phys Chem* 2019;93:730-5. DOI
58. Tarachand, Hussain S, Lalla NP, et al. Thermoelectric properties of Ag-doped CuS nanocomposites synthesized by a facile polyol method. *Phys Chem Chem Phys* 2018;20:5926-35. DOI
59. Yao J, Deng B, Ellis DE, Ibers JA. Syntheses, structures, physical properties, and electronic structures of KLn_2CuS_4 (Ln = Y, Nd, Sm, Tb, Ho) and $K_2Ln_4Cu_4S_9$ (Ln=Dy, Ho). *J Solid State Chem* 2003;176:5-12. DOI
60. Roo J. Chemical Considerations for Colloidal Nanocrystal Synthesis. *Chem Mater* 2022;34:5766-79. DOI

61. Rachkov AG, Schimpf AM. Colloidal Synthesis of Tunable Copper Phosphide Nanocrystals. *Chem Mater* 2021;33:1394-406. DOI
62. Doan-Nguyen TP, Jiang S, Koynov K, Landfester K, Crespy D. Ultrasmall Nanocapsules Obtained by Controlling Ostwald Ripening. *Angew Chem Int Ed Engl* 2021;60:18094-102. DOI PubMed
63. Wu J, Zhang Z, Fang Y, et al. Plasmon-enhanced photocatalytic cumulative effect on 2D semiconductor heterojunctions towards highly-efficient visible-light-driven solar-to-fuels conversion. *J Chem Eng* 2022;437:135308. DOI
64. Wang W, Fang J, Huang X. Different behaviors between interband and intraband transitions generated hot carriers on g-C_3N_4/Au for photocatalytic H_2 production. *Appl Sur Sci* 2020;513:145830. DOI
65. Nishi H, Tatsuma T. Electrochemical and Photoelectrochemical Applications of Plasmonic Metal and Compound Nanoparticles. *Electrochemistry* 2019;87:321-7. DOI
66. Yan C, Tian Q, Yang S. Recent advances in the rational design of copper chalcogenide to enhance the photothermal conversion efficiency for the photothermal ablation of cancer cells. *RSC Adv* 2017;7:37887-97. DOI
67. Kriegel I, Jiang C, Rodríguez-Fernández J, et al. Tuning the excitonic and plasmonic properties of copper chalcogenide nanocrystals. *J Am Chem Soc* 2012;134:1583-90. DOI
68. Chen L, Sakamoto M, Haruta M, et al. Tin Ion Directed Morphology Evolution of Copper Sulfide Nanoparticles and Tuning of Their Plasmonic Properties via Phase Conversion. *Langmuir* 2016;32:7582-7. DOI
69. Bekenstein Y, Vinokurov K, Keren-Zur S, et al. Thermal doping by vacancy formation in copper sulfide nanocrystal arrays. *Nano Lett* 2014;14:1349-53. DOI
70. Ou W, Zou Y, Wang K, et al. Active manipulation of NIR plasmonics: the case of $Cu_{2-x}Se$ through electrochemistry. *J Phys Chem Lett* 2018;9:274-80. DOI PubMed
71. Schimpf AM, Knowles KE, Carroll GM, Gamelin DR. Electronic doping and redox-potential tuning in colloidal semiconductor nanocrystals. *Acc Chem Res* 2015;48:1929-37. DOI PubMed
72. Jain PK, Manthiram K, Engel JH, White SL, Faucheaux JA, Alivisatos AP. Doped nanocrystals as plasmonic probes of redox chemistry. *Angew Chem Int Ed Engl* 2013;52:13671-5. DOI PubMed
73. Alam R, Labine M, Karwacki CJ, Kamat PV. Modulation of $Cu_{2-x}S$ nanocrystal plasmon resonance through reversible photoinduced electron transfer. *ACS Nano* 2016;10:2880-6. DOI PubMed
74. Liu K, Liu K, Liu J, et al. Copper chalcogenide materials as photothermal agents for cancer treatment. *Nanoscale* 2020;12:2902-13. DOI
75. Li J, Zhang Y, Zhang J, et al. Chemical vapor deposition of quaternary 2D BiCuSeO p-type semiconductor with intrinsic degeneracy. *Adv Mater* 2022;34:e2207796. DOI PubMed
76. Wang Y, Zhang A, Shao Z, et al. High-performance se-based photoelectrochemical photodetectors via in situ grown microrod arrays. *Adv Opt Mater* 2022;10:2201926. DOI
77. Prominski A, Shi J, Li P, et al. Porosity-based heterojunctions enable leadless optoelectronic modulation of tissues. *Nat Mater* 2022;21:647-55. DOI
78. Zhu D, Tang A, Peng L, Liu Z, Yang C, Teng F. Tuning the plasmonic resonance of $Cu_{2-x}S$ nanocrystals: effects of the crystal phase, morphology and surface ligands. *J Mater Chem C* 2016;4:4880-8. DOI
79. Liu Y, Liu M, Swihart MT. Reversible crystal phase interconversion between covellite cus and high chalcocite Cu_2S nanocrystals. *Chem Mater* 2017;29:4783-91. DOI
80. Li W, Zamani R, Rivera Gil P, et al. CuTe nanocrystals: shape and size control, plasmonic properties, and use as SERS probes and photothermal agents. *J Am Chem Soc* 2013;135:7098-101. DOI
81. De Trizio L, Li H, Casu A, et al. Sn cation valency dependence in cation exchange reactions involving $Cu_{2-x}Se$ nanocrystals. *J Am Chem Soc* 2014;136:16277-84. DOI PubMed PMC
82. Dorfs D, Härtling T, Miszta K, et al. Reversible tunability of the near-infrared valence band plasmon resonance in $Cu_{2-x}Se$ nanocrystals. *J Am Chem Soc* 2011;133:11175-80. DOI PubMed
83. Chen L, Sakamoto M, Sato R, Teranishi T. Determination of a localized surface plasmon resonance mode of Cu_7S_4 nanodisks by plasmon coupling. *Faraday Discuss* 2015;181:355-64. DOI PubMed
84. Ji M, Xu M, Zhang W, et al. Structurally well-defined Au@$Cu_{2-x}S$ core-shell nanocrystals for improved cancer treatment based on enhanced photothermal efficiency. *Adv Mater* 2016;28:3094-101. DOI PubMed
85. Zhu D, Liu M, Liu X, Liu Y, Prasad PN, Swihart MT. Au-$Cu_{2-x}Se$ heterogeneous nanocrystals for efficient photothermal heating for cancer therapy. *J Mater Chem B* 2017;5:4934-42. DOI
86. Ma L, Liang S, Liu X, Yang D, Zhou L, Wang Q. Synthesis of dumbbell-like gold-metal sulfide core-shell nanorods with largely enhanced transverse plasmon resonance in visible region and efficiently improved photocatalytic activity. *Adv Funct Mater* 2015;25:898-904. DOI
87. Liu X, Lee C, Law WC, et al. Au-$Cu_{2-x}Se$ heterodimer nanoparticles with broad localized surface plasmon resonance as contrast agents for deep tissue imaging. *Nano Lett* 2013;13:4333-9. DOI PubMed
88. Liu JN, Bu W, Shi J. Chemical design and synthesis of functionalized probes for imaging and treating tumor hypoxia. *Chem Rev* 2017;117:6160-224. DOI PubMed
89. Liu Y, Ai K, Liu J, Deng M, He Y, Lu L. Dopamine-melanin colloidal nanospheres: an efficient near-infrared photothermal therapeutic agent for in vivo cancer therapy. *Adv Mater* 2013;25:1353-9. DOI
90. Tian Q, Tang M, Sun Y, et al. Hydrophilic flower-like CuS superstructures as an efficient 980 nm laser-driven photothermal agent for

ablation of cancer cells. *Adv Mater* 2011;23:3542-7. DOI

91. Kriegel I, Scotognella F, Manna L. Plasmonic doped semiconductor nanocrystals: Properties, fabrication, applications and perspectives. *Phys Rep* 2017;674:1-52. DOI
92. Fenton JL, Schaak RE. Structure-selective cation exchange in the synthesis of zincblende MnS and CoS nanocrystals. *Angew Chem Int Ed Engl* 2017;56:6464-7. DOI PubMed
93. Coughlan C, Ibáñez M, Dobrozhan O, Singh A, Cabot A, Ryan KM. Compound copper chalcogenide nanocrystals. *Chem Rev* 2017;117:5865-6109. DOI PubMed
94. Balendhran S, Hussain Z, Shrestha VR, et al. Copper tetracyanoquinodimethane (CuTCNQ): a metal-organic semiconductor for room-temperature visible to long-wave infrared photodetection. *ACS Appl Mater Interfaces* 2021;13:38544-52. DOI PubMed
95. Muhammad Z, Mu K, Lv H, et al. Electron doping induced semiconductor to metal transitions in $ZrSe_2$ layers via copper atomic intercalation. *Nano Res* 2018;11:4914-22. DOI
96. Gan Z, Zhou P, Dong A, Zheng D, Wang H. A laser and electric pulse modulated nonvolatile photoelectric response in nanoscale copper dusted metal-oxide-semiconductor structures. *Adv Electron Mater* 2018;4:1800234. DOI
97. Muhammed MA, Döblinger M, Rodríguez-Fernández J. Switching plasmons: gold nanorod-copper chalcogenide core-shell nanoparticle clusters with selectable metal/semiconductor NIR plasmon resonances. *J Am Chem Soc* 2015;137:11666-77. DOI PubMed
98. Linic S, Christopher P, Ingram DB. Plasmonic-metal nanostructures for efficient conversion of solar to chemical energy. *Nat Mater* 2011;10:911-21. DOI PubMed
99. Ma RM, Oulton RF, Sorger VJ, Bartal G, Zhang X. Room-temperature sub-diffraction-limited plasmon laser by total internal reflection. *Nat Mater* 2011;10:110-3. DOI PubMed
100. Alavirad M, Roy L, Berini P. Surface plasmon enhanced photodetectors based on internal photoemission. *J Photon Energy* 2016;6:042511. DOI
101. Fang Y, Jiao Y, Xiong K, et al. Plasmon enhanced internal photoemission in antenna-spacer-mirror based Au/TiO_2 nanostructures. *Nano Lett* 2015;15:4059-65. DOI PubMed
102. Smith JG, Faucheaux JA, Jain PK. Plasmon resonances for solar energy harvesting: a mechanistic outlook. *Nano Today* 2015;10:67-80. DOI
103. Zhou D, Li D, Zhou X, et al. Semiconductor plasmon induced up-conversion enhancement in m$Cu_{2-x}S$@SiO_2@Y_2O_3:Yb^{3+}/Er^{3+} core-shell nanocomposites. *ACS Appl Mater Interfaces* 2017;9:35226-33. DOI PubMed
104. Cui J, Xu S, Guo C, Jiang R, James TD, Wang L. Highly efficient photothermal semiconductor nanocomposites for photothermal imaging of latent fingerprints. *Anal Chem* 2015;87:11592-8. DOI
105. Cui J, Jiang R, Guo C, Bai X, Xu S, Wang L. Fluorine grafted Cu_7S_4-Au heterodimers for multimodal imaging guided photothermal therapy with high penetration depth. *J Am Chem Soc* 2018;140:5890-4. DOI
106. Wang Y, Wang W, Sang D, Yu K, Lin H, Qu F. $Cu_{2-x}Se$/Bi_2Se_3@PEG Z-scheme heterostructure: a multimode bioimaging guided theranostic agent with enhanced photo/chemodynamic and photothermal therapy. *Biomater Sci* 2021;9:4473-83. DOI PubMed
107. Shi H, Yan R, Wu L, et al. Tumor-targeting CuS nanoparticles for multimodal imaging and guided photothermal therapy of lymph node metastasis. *Acta Biomater* 2018;72:256-65. DOI
108. Yuan Y, Raj P, Zhang J, Siddhanta S, Barman I, Bulte JWM. Furin-mediated self-assembly of olsalazine nanoparticles for targeted raman imaging of tumors. *Angew Chem Int Ed Engl* 2021;60:3923-7. DOI PubMed PMC
109. Lee S, Pham TC, Bae C, Choi Y, Kim YK, Yoon J. Nano theranostics platforms that utilize proteins. *Coord Chem Rev* 2020;412:213258. DOI
110. Cai H, Dai X, Wang X, et al. A nanostrategy for efficient imaging-guided antitumor therapy through a stimuli-responsive branched polymeric prodrug. *Adv Sci* 2020;7:1903243. DOI PubMed PMC
111. Staal AHJ, Becker K, Tagit O, et al. In vivo clearance of ^{19}F MRI imaging nanocarriers is strongly influenced by nanoparticle ultrastructure. *Biomaterials* 2020;261:120307. DOI PubMed
112. Su H, Kwok KW, Cleary K, et al. State of the art and future opportunities in MRI-guided robot-assisted surgery and interventions. *Proc IEEE Inst Electr Electron Eng* 2022;110:968-92. DOI PubMed PMC
113. Xu J, Zhang Y, Liu Y, et al. Vitality-enhanced dual-modal tracking system reveals the dynamic fate of mesenchymal stem cells for stroke therapy. *Small* 2022;18:e2203431. DOI PubMed
114. Wang H, Wang Y, Lu L, et al. Reducing valence states of Co Active Sites in a Single-Atom Nanozyme for Boosted Tumor Therapy. *Adv Funct Materials* 2022;32:2200331. DOI
115. Pipal RW, Stout KT, Musacchio PZ, et al. Metallaphotoredox aryl and alkyl radiomethylation for PET ligand discovery. *Nature* 2021;589:542-7. DOI PubMed PMC
116. Chen Y, Zhao B, Zhang H, Zhang T, Yang D, Qiu F. Laminated PET-based membranes with sweat transportation and dual thermal insulation properties. *J Chem Eng* 2022;450:138177. DOI
117. Zhou YP, Sun Y, Takahashi K, et al. Development of a PET radioligand for α2δ-1 subunit of calcium channels for imaging neuropathic pain. *Eur J Med Chem* 2022;242:114688. DOI PubMed PMC
118. Wu W, Pu Y, Shi J. Dual Size/charge-switchable nanocatalytic medicine for deep tumor therapy. *Adv Sci* 2021;8:2002816. DOI PubMed PMC
119. Guo W, Sun X, Jacobson O, et al. Intrinsically radioactive [^{64}Cu]CuInS/ZnS quantum dots for PET and optical imaging: improved

radiochemical stability and controllable Cerenkov luminescence. *ACS Nano* 2015;9:488-95. DOI PubMed PMC

120. Zhou M, Zhang R, Huang M, et al. A chelator-free multifunctional [^{64}Cu]CuS nanoparticle platform for simultaneous micro-PET/CT imaging and photothermal ablation therapy. *J Am Chem Soc* 2010;132:15351-8. DOI PubMed PMC
121. Quintana C, Cifuentes MP, Humphrey MG. Transition metal complex/gold nanoparticle hybrid materials. *Chem Soc Rev* 2020;49:2316-41. DOI PubMed
122. Shin TH, Choi Y, Kim S, Cheon J. Recent advances in magnetic nanoparticle-based multi-modal imaging. *Chem Soc Rev* 2015;44:4501-16. DOI
123. Chen Y, Liu X, Wu R, Cui J, Hu G, Wang L. Dual active center-assembled $Cu_{31}S_{16}$-$Co_{9-x}Ni_xS_8$ heterodimers: coherent interface engineering induces multihole accumulation for light-enhanced electrocatalytic oxygen evolution. *ACS Appl Mater Interfaces* 2021;13:20094-104. DOI PubMed
124. Xu J, Cui J, Guo C, et al. Ultrasmall Cu_7S_4 @MoS_2 Hetero-nanoframes with abundant active edge sites for ultrahigh-performance hydrogen evolution. *Angew Chem Int Ed Engl* 2016;55:6502-5. DOI PubMed
125. Zhu H, Zhou Y, Wang Y, Xu S, James TD, Wang L. Stepwise-enhanced tumor targeting of near-infrared emissive Au Nanoclusters with high quantum yields and long-term stability. *Anal Chem* 2022;94:13189-96. DOI PubMed PMC
126. Shi H, Sun Y, Yan R, et al. Magnetic semiconductor Gd-doping CuS nanoparticles as activatable nanoprobes for bimodal imaging and targeted photothermal therapy of gastric tumors. *Nano Lett* 2019;19:937-47. DOI
127. Han Y, Wang T, Liu H, et al. The release and detection of copper ions from ultrasmall theranostic $Cu_{2-x}Se$ nanoparticles. *Nanoscale* 2019;11:11819-29. DOI PubMed
128. Zhang Y, Fang J, Ye S, et al. A hydrogen sulphide-responsive and depleting nanoplatform for cancer photodynamic therapy. *Nat Commun* 2022;13:1685. DOI PubMed PMC
129. Cui C, Li J, Fang J, et al. Building multipurpose nano-toolkit by rationally decorating NIR-II fluorophore to meet the needs of tumor diagnosis and treatment. *Chin Chem Lett* 2022;33:3478-83. DOI
130. Zhao M, Ding J, Mao Q, et al. A novel $\alpha_v\beta_3$ integrin-targeted NIR-II nanoprobe for multimodal imaging-guided photothermal therapy of tumors *in vivo*. *Nanoscale* 2020;12:6953-8. DOI
131. Yun B, Zhu H, Yuan J, Sun Q, Li Z. Synthesis, modification and bioapplications of nanoscale copper chalcogenides. *J Mater Chem B* 2020;8:4778-812. DOI
132. Sarma A, Gutowski O, Seeck O, et al. Photothermal synthesis of copper sulfide nanowires for direct lithography of chalcogenides on a chip. *ACS Appl Nano Mater* 2022;5:4367-75. DOI
133. Li Y, Lu W, Huang Q, Huang M, Li C, Chen W. Copper sulfide nanoparticles for photothermal ablation of tumor cells. *Nanomedicine* 2010;5:1161-71. DOI
134. Zhou M, Li J, Liang S, Sood AK, Liang D, Li C. CuS nanodots with ultrahigh efficient renal clearance for positron emission tomography imaging and image-guided photothermal therapy. *ACS Nano* 2015;9:7085-96. DOI PubMed PMC
135. Zhang S, Sun C, Zeng J, et al. Ambient aqueous synthesis of ultrasmall PEGylated $Cu_{2-x}Se$ nanoparticles as a multifunctional theranostic agent for multimodal imaging guided photothermal therapy of cancer. *Adv Mater* 2016;28:8927-36. DOI PubMed
136. Bao J, Wang Y, Li C, et al. Gold-promoting-satellite to boost photothermal conversion efficiency of $Cu_{2-x}Se$ for triple-negative breast cancer targeting therapy. *Materials Today Nano* 2022;18:100211. DOI
137. Chen H, Song M, Tang J, et al. Ultrahigh ^{19}F loaded $Cu_{1.75}S$ nanoprobes for simultaneous (19)F magnetic resonance imaging and photothermal therapy. *ACS Nano* 2016;10:1355-62. DOI PubMed PMC
138. Guo C, Yan Y, Xu S, Wang L. In situ fabrication of nanoprobes for ^{19}F magnetic resonance and photoacoustic imaging-guided tumor therapy. *Anal Chem* 2022;94:5317-24. DOI PubMed
139. Huang X, Zhang W, Guan G, Song G, Zou R, Hu J. Design and functionalization of the NIR-responsive photothermal semiconductor nanomaterials for cancer theranostics. *Acc Chem Res* 2017;50:2529-38. DOI
140. Siegel RL, Miller KD, Fuchs HE, Jemal A. Cancer statistics for the US Hispanic/Latino population, 2021. *CA Cancer J Clin* 2021;71:7-33. DOI PubMed
141. Cho NH, Cheong TC, Min JH, et al. A multifunctional core-shell nanoparticle for dendritic cell-based cancer immunotherapy. *Nat Nanotechnol* 2011;6:675-82. DOI PubMed
142. Li J, Ge Z, Toh K, et al. Enzymatically transformable polymersome-based nanotherapeutics to eliminate minimal relapsable cancer. *Adv Mater* 2021;33:e2105254. DOI PubMed
143. Izci M, Maksoudian C, Manshian BB, Soenen SJ. The use of alternative strategies for enhanced nanoparticle delivery to solid tumors. *Chem Rev* 2021;121:1746-803. DOI PubMed PMC
144. Ding J, Mao Q, Zhao M, et al. Protein sulfenic acid-mediated anchoring of gold nanoparticles for enhanced CT imaging and radiotherapy of tumors *in vivo*. *Nanoscale* 2020;12:22963-9. DOI PubMed
145. Mao Q, Fang J, Wang A, et al. Aggregation of gold nanoparticles triggered by hydrogen peroxide-initiated chemiluminescence for activated tumor theranostics. *Angew Chem Int Ed Engl* 2021;60:23805-11. DOI PubMed
146. Fang J, Zhao Y, Wang A, et al. In vivo quantitative assessment of a radiation dose based on ratiometric photoacoustic imaging of tumor apoptosis. *Anal Chem* 2022;94:5149-58. DOI
147. Ye S, Cui C, Cheng X, et al. Red light-initiated cross-linking of NIR probes to cytoplasmic RNA: an innovative strategy for prolonged imaging and unexpected tumor suppression. *J Am Chem Soc* 2020;142:21502-12. DOI
148. Cui J, Jiang R, Lu W, Xu S, Wang L. Plasmon-enhanced photoelectrical hydrogen evolution on monolayer MoS_2 decorated $Cu_{1.75}S$-

Au nanocrystals. *Small* 2017;13:1602235. DOI PubMed

149. Cheng Y, Chen Q, Guo Z, et al. An Intelligent biomimetic nanoplatform for holistic treatment of metastatic triple-negative breast cancer *via* photothermal ablation and immune remodeling. *ACS Nano* 2020;14:15161-81. DOI PubMed
150. Song G, Wang Q, Wang Y, et al. A low-toxic multifunctional nanoplatform based on Cu_9S_5@mSiO_2 core-shell nanocomposites: combining photothermal- and chemotherapies with infrared thermal imaging for cancer treatment. *Adv Funct Mater* 2013;23:4281-92. DOI
151. Zhou M, Chen Y, Adachi M, et al. Single agent nanoparticle for radiotherapy and radio-photothermal therapy in anaplastic thyroid cancer. *Biomaterials* 2015;57:41-9. DOI PubMed PMC
152. Lin LS, Huang T, Song J, et al. Synthesis of copper peroxide nanodots for H_2O_2 self-supplying chemodynamic therapy. *J Am Chem Soc* 2019;141:9937-45. DOI PubMed
153. Wang R, He Z, Cai P, et al. Surface-functionalized modified copper sulfide nanoparticles enhance checkpoint blockade tumor immunotherapy by photothermal therapy and antigen capturing. *ACS Appl Mater Interfaces* 2019;11:13964-72. DOI
154. Shen S, Gao Y, Ouyang Z, Jia B, Shen M, Shi X. Photothermal-triggered dendrimer nanovaccines boost systemic antitumor immunity. *J Control Release* 2023;355:171-83. DOI PubMed
155. Wang W, Ma E, Tao P, et al. Chemical-NIR dual-powered CuS/Pt nanomotors for tumor hypoxia modulation, deep tumor penetration and augmented synergistic phototherapy. *J Mater Sci Technol* 2023;148:171-85. DOI
156. Chen Y, Liu P, Zhou C, et al. Gold nanobipyramid@copper sulfide nanotheranostics for image-guided NIR-II photo/chemodynamic cancer therapy with enhanced immune response. *Acta Biomater* 2023;158:649-59. DOI
157. Gao F, Jiang L, Zhang J, et al. Near-infrared light-responsive nanosystem with prolonged circulation and enhanced penetration for increased photothermal and photodynamic therapy. *ACS Materials Lett* 2023;5:1-10. DOI
158. Liang J, Niu M, Luo G, et al. Tailor-made biotuner against colorectal tumor microenvironment to transfer harms into treasures for synergistic oncotherapy. *Nano Today* 2022;47:101662. DOI
159. Yang G, Li M, Song T, et al. Polydopamine-engineered theranostic nanoscouts enabling intracellular HSP90 mRNAs Fluorescence detection for imaging-guided chemo-photothermal therapy. *Adv Healthc Mater* 2022;11:e2201615. DOI PubMed
160. Xin Y, Guo Z, Ma A, et al. A robust ROS generation nanoplatform combating periodontitis via sonodynamic/chemodynamic combination therapy. *J Chem Eng* 2023;451:138782. DOI
161. Zhang H, Han R, Song P, et al. Hydrogen peroxide self-sufficient and glutathione-depleted nanoplatform for boosting chemodynamic therapy synergetic phototherapy. *J Colloid Interface Sci* 2023;629:103-13. DOI
162. Shi Z, Tang J, Lin C, et al. Construction of iron-mineralized black phosphorene nanosheet to combinate chemodynamic therapy and photothermal therapy. *Drug Deliv* 2022;29:624-36. DOI PubMed PMC
163. Chen ZA, Li ZH, Li CJ, et al. Manganese-containing polydopamine nanoparticles as theranostic agents for magnetic resonance imaging and photothermal/chemodynamic combined ferroptosis therapy treating gastric cancer. *Drug Deliv* ;29:1201-1211. DOI PubMed PMC
164. Shi L, Wang Y, Zhang C, et al. An acidity-unlocked magnetic nanoplatform enables self-boosting ROS generation through upregulation of lactate for imaging-guided highly specific chemodynamic therapy. *Angew Chem Int Ed Engl* 2021;60:9562-72. DOI PubMed
165. Liu C, Cao Y, Cheng Y, et al. An open source and reduce expenditure ROS generation strategy for chemodynamic/photodynamic synergistic therapy. *Nat Commun* 2020;11:1735. DOI PubMed PMC
166. Deng L, Liu M, Sheng D, et al. Low-intensity focused ultrasound-augmented Cascade chemodynamic therapy via boosting ROS generation. *Biomaterials* 2021;271:120710. DOI
167. Shen J, Yu H, Shu Y, Ma M, Chen H. A robust ros generation strategy for enhanced chemodynamic/photodynamic therapy via H_2O_2/O_2 self-supply and Ca^{2+} overloading. *Adv Funct Mater* 2021;31:2106106. DOI
168. Song M, Cheng Y, Tian Y, et al. Sonoactivated chemodynamic therapy: a robust ros generation nanotheranostic eradicates multidrug-resistant bacterial infection. *Adv Funct Mater* 2020;30:2003587. DOI
169. Huang C, Wang Y, Wang Y, et al. Ultraweak chemiluminescence enhanced on the surface of lanthanide metal–organic framework nanosheets synthesized by ultrasonic wave. *Appl Surf Sci* 2022;579:151860. DOI
170. Cao Z, Zhang L, Liang K, et al. Biodegradable 2D Fe-Al hydroxide for nanocatalytic tumor-dynamic therapy with tumor specificity. *Adv Sci* 2018;5:1801155. DOI PubMed PMC
171. Li M, Xia J, Tian R, et al. Near-infrared light-initiated molecular superoxide radical generator: rejuvenating photodynamic therapy against hypoxic tumors. *J Am Chem Soc* 2018;140:14851-9. DOI
172. Wang Z, Zhang Y, Ju E, et al. Biomimetic nanoflowers by self-assembly of nanozymes to induce intracellular oxidative damage against hypoxic tumors. *Nat Commun* 2018;9:3334. DOI PubMed PMC
173. Wu W, Yu L, Jiang Q, et al. Enhanced tumor-specific disulfiram chemotherapy by in situ Cu^{2+} chelation-initiated nontoxicity-to-toxicity transition. *J Am Chem Soc* 2019;141:11531-9. DOI PubMed
174. Zuo W, Liu N, Chang Z, et al. Single-site bimetallic nanosheet for imaging guided mutually-reinforced photothermal-chemodynamic therapy. *J Chem Eng* 2022;442:136125. DOI
175. Wang S, Pang Y, Hu S, Lv J, Lin Y, Li M. Copper sulfide engineered covalent organic frameworks for pH-responsive chemo/photothermal/chemodynamic synergistic therapy against cancer. *J Chem Eng* 2023;451:138864. DOI
176. Bharathiraja S, Manivasagan P, Moorthy MS, Bui NQ, Lee KD, Oh J. Chlorin e6 conjugated copper sulfide nanoparticles for

photodynamic combined photothermal therapy. *Photodiagnosis Photodyn Ther* 2017;19:128-34. DOI PubMed

177. Nikam AN, Pandey A, Fernandes G, et al. Copper sulphide based heterogeneous nanoplatforms for multimodal therapy and imaging of cancer: Recent advances and toxicological perspectives. *Coord Chem Rev* 2020;419:213356. DOI
178. Han L, Zhang Y, Chen XW, Shu Y, Wang JH. Protein-modified hollow copper sulfide nanoparticles carrying indocyanine green for photothermal and photodynamic therapy. *J Mater Chem B* 2016;4:105-12. DOI
179. Liu W, Xiang H, Tan M, et al. Nanomedicine enables drug-potency activation with tumor sensitivity and hyperthermia synergy in the second near-infrared biowindow. *ACS Nano* 2021;15:6457-70. DOI
180. Chen L, Zhou L, Wang C, et al. Tumor-targeted drug and CpG delivery system for phototherapy and docetaxel-enhanced immunotherapy with polarization toward M1-type macrophages on triple negative breast cancers. *Adv Mater* 2019;31:e1904997. DOI PubMed
181. Ricciardi V, Portaccio M, Lasalvia M, et al. Evaluation of proton-induced biomolecular changes in MCF-10A breast cells by means of FT-IR microspectroscopy. *Appl Sci* 2022;12:5074. DOI
182. Qi J, Geng C, Tang X, et al. Effect of spatial distribution of boron and oxygen concentration on DNA damage induced from boron neutron capture therapy using Monte Carlo simulations. *Int J Radiat Biol* 2021;97:986-96. DOI
183. Ganjeh Z, Eslami-kalantari M, Ebrahimi Loushab M, Mowlavi AA. Calculation of direct DNA damages by a new approach for carbon ions and protons using Geant4-DNA. *Radiat Phys and Chem* 2021;179:109249. DOI
184. Zhao Y, Chen BQ, Kankala RK, Wang SB, Chen AZ. Recent advances in combination of copper chalcogenide-based photothermal and reactive oxygen species-related therapies. *ACS Biomater Sci Eng* 2020;6:4799-815. DOI
185. Zhou X, Liu H, Zheng Y, et al. Overcoming radioresistance in tumor therapy by alleviating hypoxia and using the HIF-1 inhibitor. *ACS Appl Mater Interfaces* 2020;12:4231-40. DOI
186. Peng C, Liang Y, Chen Y, et al. Hollow mesoporous tantalum oxide based nanospheres for triple sensitization of radiotherapy. *ACS Appl Mater Interfaces* 2020;12:5520-30. DOI
187. Jiang W, Han X, Zhang T, Xie D, Zhang H, Hu Y. An oxygen self-evolving, multistage delivery system for deeply located hypoxic tumor treatment. *Adv Healthc Mater* 2020;9:e1901303. DOI PubMed
188. Yan T, Yang K, Chen C, et al. Synergistic photothermal cancer immunotherapy by Cas9 ribonucleoprotein-based copper sulfide nanotherapeutic platform targeting PTPN2. *Biomaterials* 2021;279:121233. DOI
189. Li N, Sun Q, Yu Z, et al. Nuclear-targeted photothermal therapy prevents cancer recurrence with near-infrared triggered copper sulfide nanoparticles. *ACS Nano* 2018;12:5197-206. DOI
190. Jiang Y, Huo Z, Qi X, Zuo T, Wu Z. Copper-induced tumor cell death mechanisms and antitumor theragnostic applications of copper complexes. *Nanomedicine* 2022;17:303-24. DOI PubMed
191. Kahlson MA, Dixon SJ. Copper-induced cell death. *Science* 2022;375:1231-2. DOI PubMed